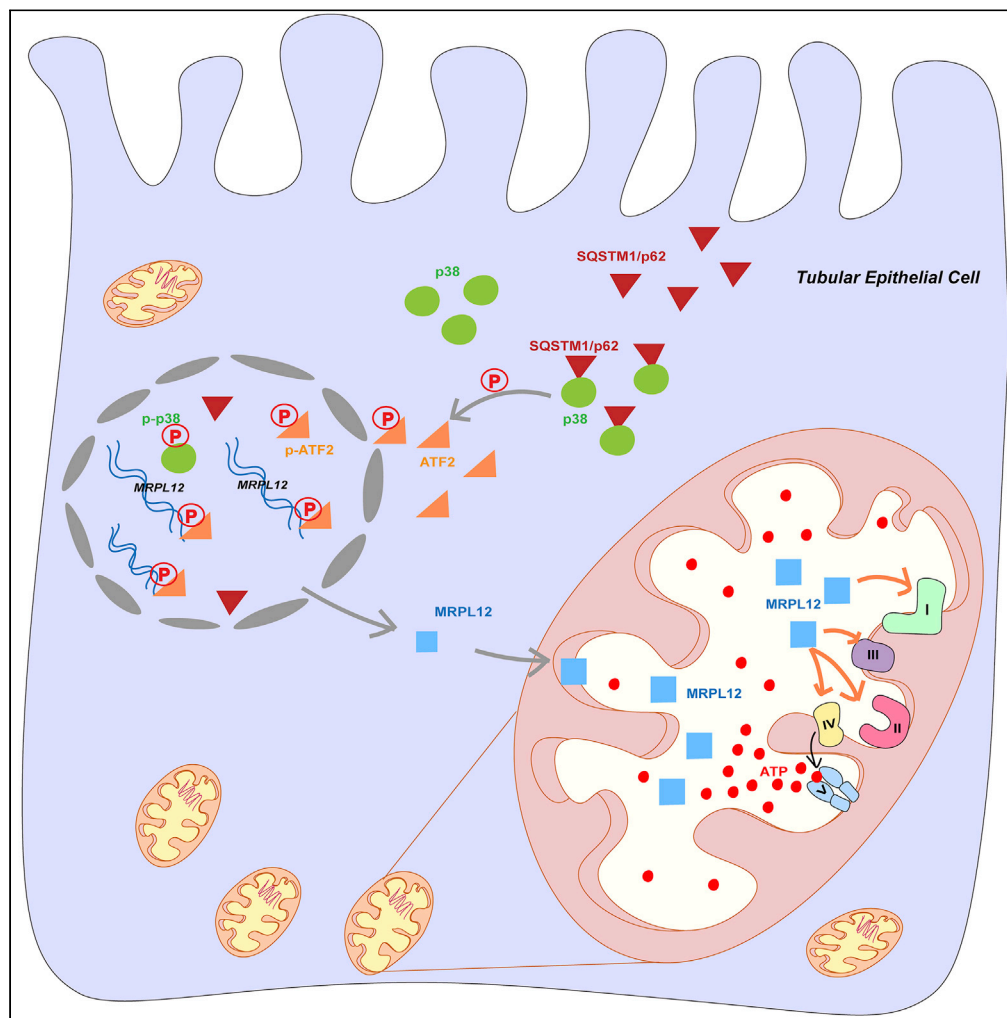**Article**

SQSTM1/p62 Controls mtDNA Expression and Participates in Mitochondrial Energetic Adaption via MRPL12

Yuan Ma, Suwei Zhu, Tingting Lv, ..., Junhui Zhen, Wei Xin, Qiang Wan

vivienxin@126.com (W.X.)
wanqiang@sdu.edu.cn (Q.W.)

HIGHLIGHTS

SQSTM1/p62 is an important regulator of mtDNA expression machinery

SQSTM1/p62 induces MRPL12 expression via activating p38/ATF2 signaling pathway

SQSTM1/p62 maintains TECs mitochondrial homeostasis and kidney function

iScience

Article

SQSTM1/p62 Controls mtDNA Expression and Participates in Mitochondrial Energetic Adaption via MRPL12

Yuan Ma,[1,8] Suwei Zhu,[2,8] Tingting Lv,[2] Xia Gu,[2] Hong Feng,[3] Junhui Zhen,[4] Wei Xin,[5,6,*] and Qiang Wan[7,9,*]

SUMMARY

Mitochondrial DNA (mtDNA) encodes thirteen core components of OXPHOS complexes, and its steady expression is crucial for cellular energy homeostasis. However, the regulation of mtDNA expression machinery, along with its sensing mechanism to energetic stresses, is not fully understood. Here, we identified SQSTM1/p62 as an important regulator of mtDNA expression machinery, which could effectively induce mtDNA expression and the effects were mediated by p38-dependent upregulation of mitochondrial ribosomal protein L12 (MRPL12) in renal tubular epithelial cells (TECs), a highly energy-demanding cell type related to OXPHOS. We further identified a direct binding site within the MRPL12 promoter to ATF2, the downstream effector of p38. Besides, SQSTM1/p62-induced mtDNA expression is involved in both serum deprivation and hypoxia-induced mitochondrial response, which was further highlighted by kidney injury phenotype of TECs-specific SQSTM1/p62 knockout mice. Collectively, these data suggest that SQSTM1/p62 is a key regulator and energetic sensor of mtDNA expression machinery.

INTRODUCTION

A major biological function of mitochondria is to provide energy in the form of ATP via oxidative phosphorylation (OXPHOS) (Cheng and Ristow, 2013). To maintain cellular energy homeostasis, the efficiency of mitochondrial OXPHOS must be under dedicated regulation to match different environmental or biological stresses, such as the changing nutrient availability and energy demands (Nunnari and Suomalainen, 2012; Gustafsson et al., 2016; Barshad et al., 2018a, 2018b). In this sense, the steady expression of the components constituting OXPHOS system, along with the fine-tuned adjustment in response to environmental challenges, is essential. The mammalian OXPHOS system is composed of about 90 proteins, among which 13 core constitutes of respiratory chain complexes are encoded by mitochondrial DNA (mtDNA) (Koc and Koc, 2012). During the past decades, the gene expression process of mtDNA has received extensive investigation, including the structure and inheritance of the mitochondrial genome, the modes of transcription and translation, and the coordinating pattern between nuclear-encoded and mitochondria-encoded genes (Nunnari and Suomalainen, 2012; Macao et al., 2015). However, modulators of mtDNA expression machinery, along with its adapting mechanisms to environmental challenges, have not been fully elucidated. To date, only a limited number of regulators have been identified. For example, PPARγ co-activator α (PGC1α) was shown to control mtDNA transcription by sensing cellular fluctuations of NAD+/NADH and AMP/ATP ratios (Bhargava and Schnellmann, 2017). NRF-1 and NRF-2 (GABP) could regulate expression of almost all complexes in the ETC (Scarpulla, 2008; Satoh et al., 2013). Besides, decreased TFAM protein levels in mitochondrial led to energetic defects and decreased mtDNA copy number, which is associated with a loss of SQSTM1/p62 (Seibenhener et al., 2013). In consideration of the complexity and plurality of energetic stresses that cells might encounter, it is reasonable to hypothesize that ample unknown regulators of mtDNA expression machinery are awaiting identification.

SQSTM1/p62, a 62-kDa protein widely expressed across different tissue types, is one of the first identified autophagy adaptors owing to its binding capability of ubiquitin and autophagy substrates, via its ubiquitin-associated domain and LC3-interacting region, respectively, which could control mitochondrial turnover via mediating mitophagy (Lamark et al., 2017). Current notions suggest that SQSTM1/p62 also harbors other functional motifs and participates in ample cellular processes, such as inflammation, tumorigenesis,

[1]Renal Division, Peking University First Hospital, Peking University Institute of Nephrology, Beijing 100034, China

[2]School of Medicine, Cheeloo College of Medicine, Shandong University, Jinan 250012, China

[3]Cancer Center, Shandong Provincial Hospital Affiliated to Shandong First Medical University, Jinan 250012, China

[4]Department of Pathology, School of Medicine, Cheeloo College of Medicine, Shandong University, Jinan 250012, China

[5]Department of Central Laboratory, Shandong Provincial Hospital, Cheeloo College of Medicine, Shandong University, Jinan 250012, China

[6]Department of Central Laboratory, Shandong Provincial Hospital Affiliated to Shandong First Medical University, Jinan 250012, China

[7]Department of Endocrinology, Shandong Provincial Hospital, Cheeloo College of Medicine, Shandong University, Jinan 250012, China

[8]These authors contributed equally

[9]Lead Contact

*Correspondence:
vivienxin@126.com (W.X.),
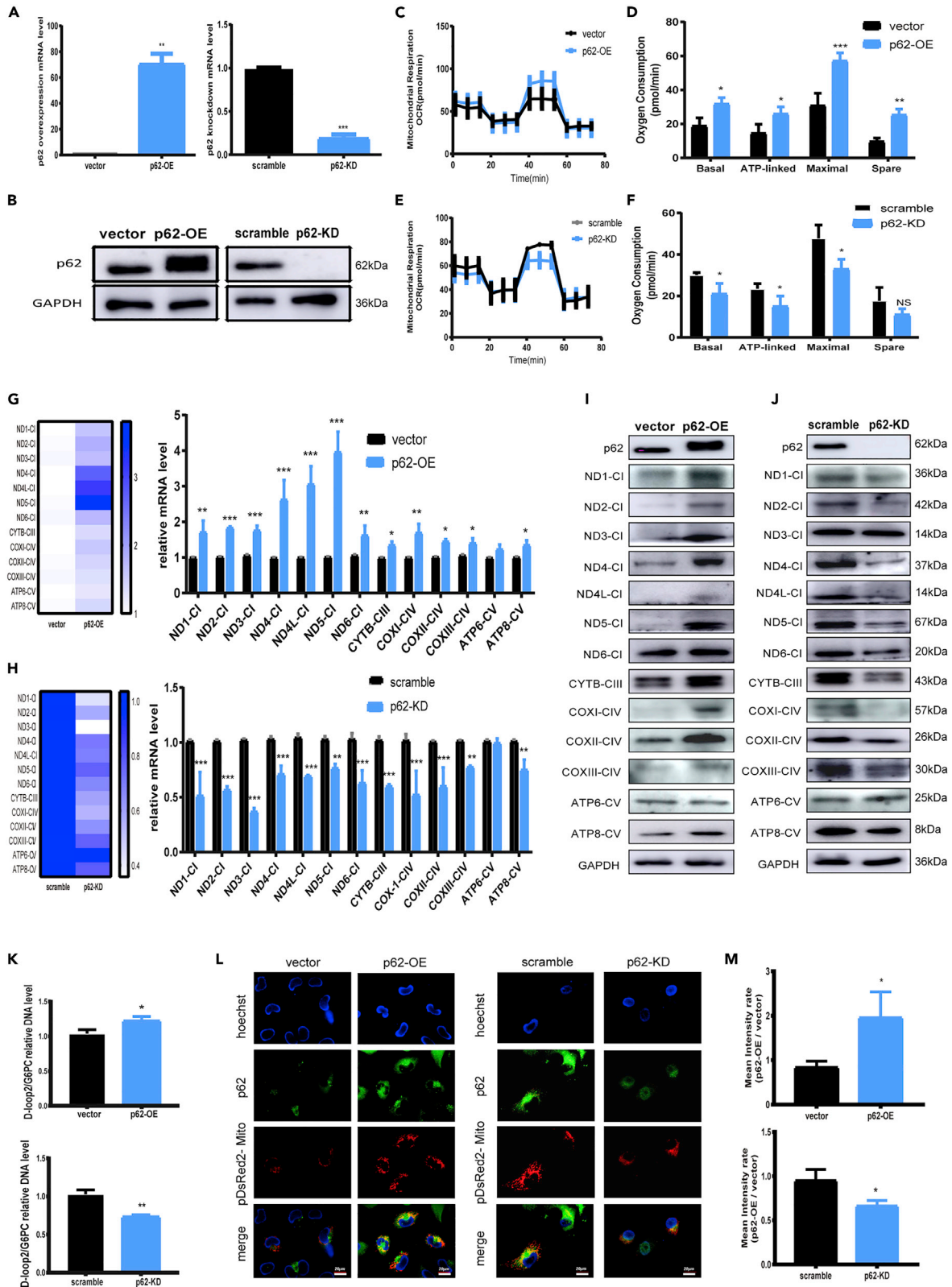wanqiang@sdu.edu.cn
(Q.W.)

Figure 1. SQSTM1/p62 Positively Regulates OXPHOS and mtDNA Expression

(A and B) qRT-PCR and western blotting showed overexpression or knockdown efficiency of SQSTM1/p62 in HK-2 cells, β-actin was used as internal control in qRT-PCR and GAPDH was used as internal control in western blotting. Unpaired, two-tailed t tests were used, n = 3, **p < 0.01, ***p < 0.001. SQSTM1/p62 was abbreviated into p62 in all figures.

(C and E) Bioenergetic profiles of HK-2 cells after SQSTM1/p62 transfection measured by Seahorse XF96.

(D and F) Mitochondrial OXPHOS were analyzed with basal respiration, ATP production, maximal respiration, and spare respiratory capacity, respectively in SQSTM1/p62 transfected HK2 cells. One-way ANOVA followed by Sidak's multiple comparisons test, n = 4 biological replicates, *p < 0.05, **p < 0.01, ***p < 0.001.

(G and H) mRNA levels of 13 mtDNA-coded OXPHOS components determined by qRT-PCR in SQSTM1/p62 transfected HK-2 cells, β-actin was used as internal control. Unpaired, two-tailed t tests were used, n = 3, *p < 0.05, **p < 0.01, ***p < 0.001. The heatmaps indicated the results of the qRT-PCR.

(I and J) Protein levels of the 13 mtDNA-coded OXPHOS components (CI: ND1 to ND6; CIII: CYTB; CIV: COXI, COXII and COXIII; CV: ATP6 and ATP8) determined by western blotting in SQSTM1/p62 transfected HK-2 cells normalized to GAPDH.

(K) mtDNA copy numbers in SQSTM1/p62-overexpressed or knocked down HK-2 cells. G6PC was used as control. Unpaired, two-tailed t tests were used, n = 3, *p < 0.05, **p < 0.01.

(L) Mitochondria abundance detected by pDsRed2-Mito plasmid transfection in SQSTM1/p62-overexpressed or knocked down cells, and the nuclei were counterstained by Hoechst 33258. Scale bars, 20 μm.

(M) Mean intensity of L was calculated by Image Pro Plus, Unpaired t tests were used, n = 3, *p < 0.05.

and metabolism (Huang et al., 2018). The role of SQSTM1/p62 in metabolism was initially highlighted by the metabolic phenotype of systemic SQSTM1/p62 knockout animals, characterized as reduced metabolic rate, mature-onset obesity, and glucose intolerance (Rodriguez et al., 2006). Further study revealed that the mechanism responsible for such phenotypes might rely on the regulation of SQSTM1/p62 on brown adipose tissue (BAT) mitochondrial thermogenesis (Muller et al., 2013). In addition, a study performed in neuroblastoma cells demonstrated SQSTM1/p62 could affect mitochondrial complex I respiration (Zhang et al., 2019). Besides, via yet-unknown mechanisms, SQSTM1/p62 could regulate the availability of NADH for electron transfer chain (ETC) (Blacker and Duchen, 2016; Bartolome et al., 2017). Another newly published data showed SQSTM1/p62 could propel metabolic reprogramming from glycolysis to mitochondrial OXPHOS during neuroepithelial stem cell differentiation (Calvo-Garrido et al., 2019). These findings suggested that SQSTM1/p62 might have autophagy-independent impacts on mitochondrial function; however, the effects seem to be tissue specific and the concrete intermediate mechanisms require further clarification.

The mammalian mitochondrial ribosome consists of associated large (39S) and small (28S) ribosomal subunits (Sharma et al., 2003), with each subunit composed of tRNAs encoded by mtDNA and multiple mitochondrial ribosomal proteins (MRPs) encoded by nuclear DNA and imported into mitochondrial matrix. Recently, several MRPs have been implicated in multiple cellular processes such as cell proliferation, apoptosis, and cell cycle regulation outside of the ribosome (Andrea et al., 2016; Cavdar Koc et al., 2001; Kashuba et al., 2008). MRPL12 is one of the best studied MRPs and was recently identified to have distinct functions in mtDNA transcription by binding to mitochondrial RNA polymerase (POLRMT) in a free form (Surovtseva et al., 2011), whereas the precise regulating mechanism remains unclear.

In the present study, we evidenced that SQSTM1/p62 could effectively control OXPHOS and mtDNA expression, which was mediated by MRPL12. The effects of SQSTM1/p62 on MRPL12 expression was in a p38/ATF2 signaling-dependent manner, with a novel binding site within the promoter of MRPL12 to ATF2 being identified. Furthermore, the regulation of SQSTM1/p62 on mtDNA expression machinery participated in both serum deprivation and hypoxia-induced mitochondrial OXPHOS response. Finally, the role of SQSTM1/p62-mediated mtDNA expression was highlighted by tubular epithelial cells (TECs)-specific SQSTM1/p62 knockout mice, which exhibited obvious kidney injury including oliguria, increased serum creatinine, and blood urea nitrogen (BUN) levels. These results suggest that SQSTM1/p62 might act as a crucial modulator and energetic sensor of mtDNA expression machinery.

RESULTS

SQSTM1/p62 Positively Controls OXPHOS and mtDNA Expression

Cellular SQSTM1/p62 contents were either elevated or reduced by transfecting SQSTM1/p62-overexpressing plasmid or silencing siRNAs, which were verified by qRT-PCR and western blotting (Figures 1A and 1B). Then cell bioenergetic profiles were analyzed using Seahorse XF96 Flux Analyzer (Figures 1C–1F). SQSTM1/p62 overexpression induced a significant elevation of basal oxygen consumption rate

(OCR), ATP-linked OCR, maximal respiration, and spare respiratory capacity, whereas SQSTM1/p62 silencing had opposite effects, suggesting SQSTM1/p62 could positively regulate mitochondrial OXPHOS.

Subsequently, we examined whether SQSTM1/p62 had impacts on mtDNA expression machinery. Transcriptional levels of thirteen mtDNA-encoded components (Figures 1G and 1H and Oligonucleotides were involved in Table S1) as well as some nDNA-encoded genes related to mitochondrial OXPHOS (Figure S1) were first determined by qRT-PCR. Overexpressing or knocking down SQSTM1/p62 induced elevations or reductions of steady-state mRNA levels of these components in various degrees, suggesting SQSTM1/p62 could positively control mtDNA expression. Western blotting analysis further confirmed the effects of SQSTM1/p62 on the protein level of these subunits (Figures 1I and 1J). Furthermore, as mtDNA transcription is known to be functionally linked to mtDNA replication (Barshad et al., 2018a, 2018b), the effects of SQSTM1/p62 on mitochondrial biogenesis were also determined. Quantification of mtDNA copy numbers (Figure 1K) and pDsRed2-Mito staining followed by intensity analysis (Figures 1L and 1M) confirmed the positive effects of SQSTM1/p62 on mitochondrial abundance. Collectively, these results clearly demonstrate that SQSTM1/p62 is a key regulator of OXPHOS and mtDNA expression coupled to mitochondrial abundance.

MRPL12 Mediates the Effects of SQSTM1/p62 on mtDNA Expression

As the effects of SQSTM1/p62 on mtDNA expression were demonstrated, we continued to explore the possible underlying mechanisms. First, we performed a mass spectrometry-based proteomics approach to screen molecules that were differentially regulated by SQSTM1/p62 knockdown. A total of 47 proteins were identified with a 95% confidence interval in SQSTM1/p62 knocked down TECs and scramble siRNA transfected control cells (Figures 2A and 2B). Of particular interest is MRPL12, with its mutations reportedly leading to mitochondrial translation deficiency (Serre et al., 2013; Frei et al., 2005). These findings propelled us to hypothesize MRPL12 as the potential molecule mediating the effects of SQSTM1/p62 on mtDNA expression. Immunostaining and western blotting were performed to verify the proteomics results. A corresponding increase or decrease of MRPL12 protein levels after SQSTM1/p62 plus or minus was evidenced (Figures 3A–3D), and the mRNA level of MRPL12 was also altered (Figure 3E), with the expression of another mitochondrial ribosome protein MRPL11 unchanged (Figure 3F), indicating SQSTM1/p62 could indeed affect MRPL12 expression specifically.

The role of MRPL12 in the regulation of SQSTM1/p62 on mitochondrial OXPHOS was then determined in TECs by dual transfection of MRPL12-silencing and SQSTM1/p62 overexpressing plasmids. As shown in Figure 3G, SQSTM1/p62-induced mitochondrial respiration was effectively diminished by additional MRPL12 knockdown, which was evaluated by basal OCR (Figure 3H), ATP-linked OCR (Figure 3I), maximal respiration (Figure 3J), and spare respiratory capacity (Figure 3K). The SQSTM1/p62-induced expression of OXPHOS complex I, III, IV, and V was also compromised by the combination of MRPL12 knockdown (Figure 3L). In addition, SQSTM1/p62 was no longer able to boost the mtDNA copy number in MRPL12-depleted cells (Figure 3M). These results clearly evidenced that SQSTM1/p62-induced mtDNA expression was mediated by MRPL12. To further address the claim, MRPL12 overexpression or knockdown cells were prepared to sufficiently induce or suppress mtDNA expression (Figures 3N and 3O). Furthermore, as MRPL12 was known to interact with mitochondrial RNA polymerase POLRMT to modulate mtDNA encoded gene expression (Surovtseva et al., 2011), we also performed co-immunoprecipitation (coIP) study, which revealed that SQSTM1/p62 plus or minus led to a corresponding elevation or reduction of POLRMT binding to MRPL12 (Figure 3P).

SQSTM1/p62 Induces MRPL12 Expression via Activating p38/ATF2 Signaling Pathway

We continued to determine how SQSTM1/p62 affected MRPL12 expression in two aspects simultaneously. On one hand, SQSTM1/p62 is known to harbor several functional motifs and could interact with molecules of multiple signaling pathways (Long et al., 2017). Accordingly, in SQSTM1/p62-overexpressed cells, specific inhibitors or activators of these pathways were employed in the following experiments, including p38 inhibitor (SB203580), Nrf2 activator (NK252), mTOR inhibitor (Rapamycin), IRS-1/2 inhibitor (NT157), Erk 1/2 activator (Honokiol), and PKC inhibitor (Go6983) (Hisatsune et al., 2008; Saito et al., 2008; Lee et al., 2010; Yang et al., 2019; Kanayama et al., 2015; Reilly et al., 2015) (Figure 4A and detail information of the reagents was listed in Table S1), and the expression of MRPL12 was evaluated by western blotting (Figure 4B). Notably, p38 inhibitor and mTOR inhibitor effectively blocked SQSTM1/p62-induced MRPL12 expression, indicating these two pathways might be involved. On the other hand, considering that MRPL12 might be regulated by SQSTM1/p62 at the transcriptional level, website: http://alggen.lsi.upc.es/cgi-bin/
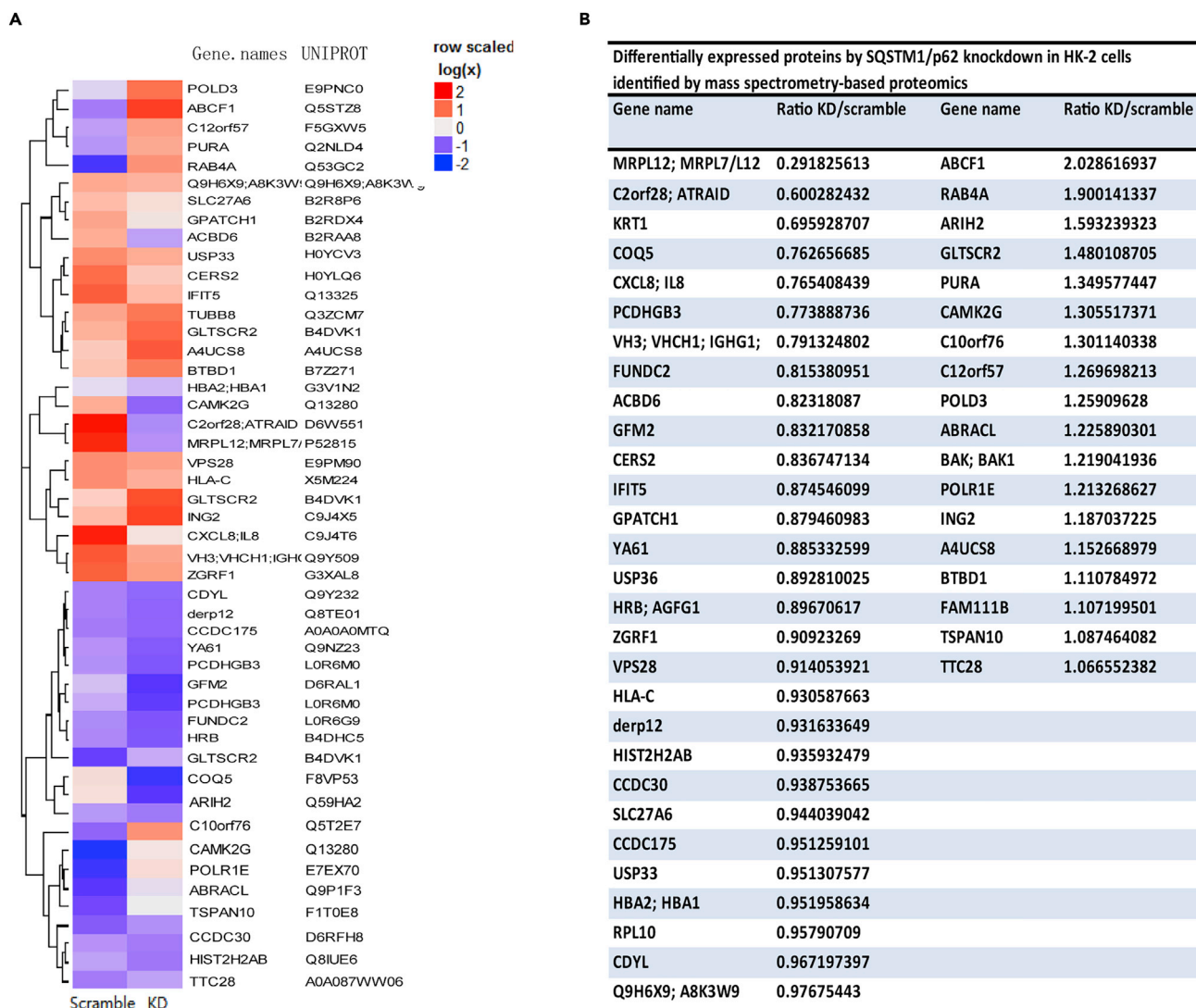
A

B

Differentially expressed proteins by SQSTM1/p62 knockdown in HK-2 cells identified by mass spectrometry-based proteomics			
Gene name	**Ratio KD/scramble**	**Gene name**	**Ratio KD/scramble**
MRPL12; MRPL7/L12	0.291825613	ABCF1	2.028616937
C2orf28; ATRAID	0.600282432	RAB4A	1.900141337
KRT1	0.695928707	ARIH2	1.593239323
COQ5	0.762656685	GLTSCR2	1.480108705
CXCL8; IL8	0.765408439	PURA	1.349577447
PCDHGB3	0.773888736	CAMK2G	1.305517371
VH3; VHCH1; IGHG1;	0.791324802	C10orf76	1.301140338
FUNDC2	0.815380951	C12orf57	1.269698213
ACBD6	0.82318087	POLD3	1.25909628
GFM2	0.832170858	ABRACL	1.225890301
CERS2	0.836747134	BAK; BAK1	1.219041936
IFIT5	0.874546099	POLR1E	1.213268627
GPATCH1	0.879460983	ING2	1.187037225
YA61	0.885332599	A4UCS8	1.152668979
USP36	0.892810025	BTBD1	1.110784972
HRB; AGFG1	0.89670617	FAM111B	1.107199501
ZGRF1	0.90923269	TSPAN10	1.087464082
VPS28	0.914053921	TTC28	1.066552382
HLA-C	0.930587663		
derp12	0.931633649		
HIST2H2AB	0.935932479		
CCDC30	0.938753665		
SLC27A6	0.944039042		
CCDC175	0.951259101		
USP33	0.951307577		
HBA2; HBA1	0.951958634		
RPL10	0.95790709		
CDYL	0.967197397		
Q9H6X9; A8K3W9	0.97675443		

Figure 2. Mass Spectrometry-Based Proteomics

(A) The heatmap of M-S analysis. A total of 47 proteins were identified with a 95% confidence interval in SQSTM1/p62 knocked down TECs and scramble siRNA transfected control cells.

(B) The ratio of 47 protein expression in p62-KD and scramble.

promo_v3/promo/promoinit.cgi?dirDB=TF_8.3/ was used to identify putative transcription factor binding sites within the MRPL12 promoter region. Among the several potential transcription factors predicted, ATF2 is known as a downstream effector of p38, with the predicted promoter binding site of −2,344 bp to −2,336 bp (Figure 4C). Thus, a potential p38/ATF2-mediated transcriptional regulating mechanism was speculated.

Subsequently, we observed the effects of SQSTM1/p62 on p38/ATF2 signaling pathway. Although SQSTM1/p62 plus or minus had no effects on the total amounts of p38 and ATF2 in cytosol (Figures 4D–4G), nuclear abundance of phosphorylated p38 (p-p38) and phosphorylated ATF2 (p-ATF2) significantly increased or decreased (Figures 4H–4K). Such results were further confirmed by immunostaining study, as nuclear p-ATF2 staining was significantly enhanced by SQSTM1/p62 overexpression and diminished by SQSTM1/p62 suppression, respectively (Figures 4L and 4M), suggesting SQSTM1/p62 could activate p38 signaling and accordingly induce p-ATF2 to translocate into the nucleus. As SQSTM1/p62 was reported to enhance p38 activity by binding to p38 (Sudo et al., 2000; Saito et al., 2008), we further
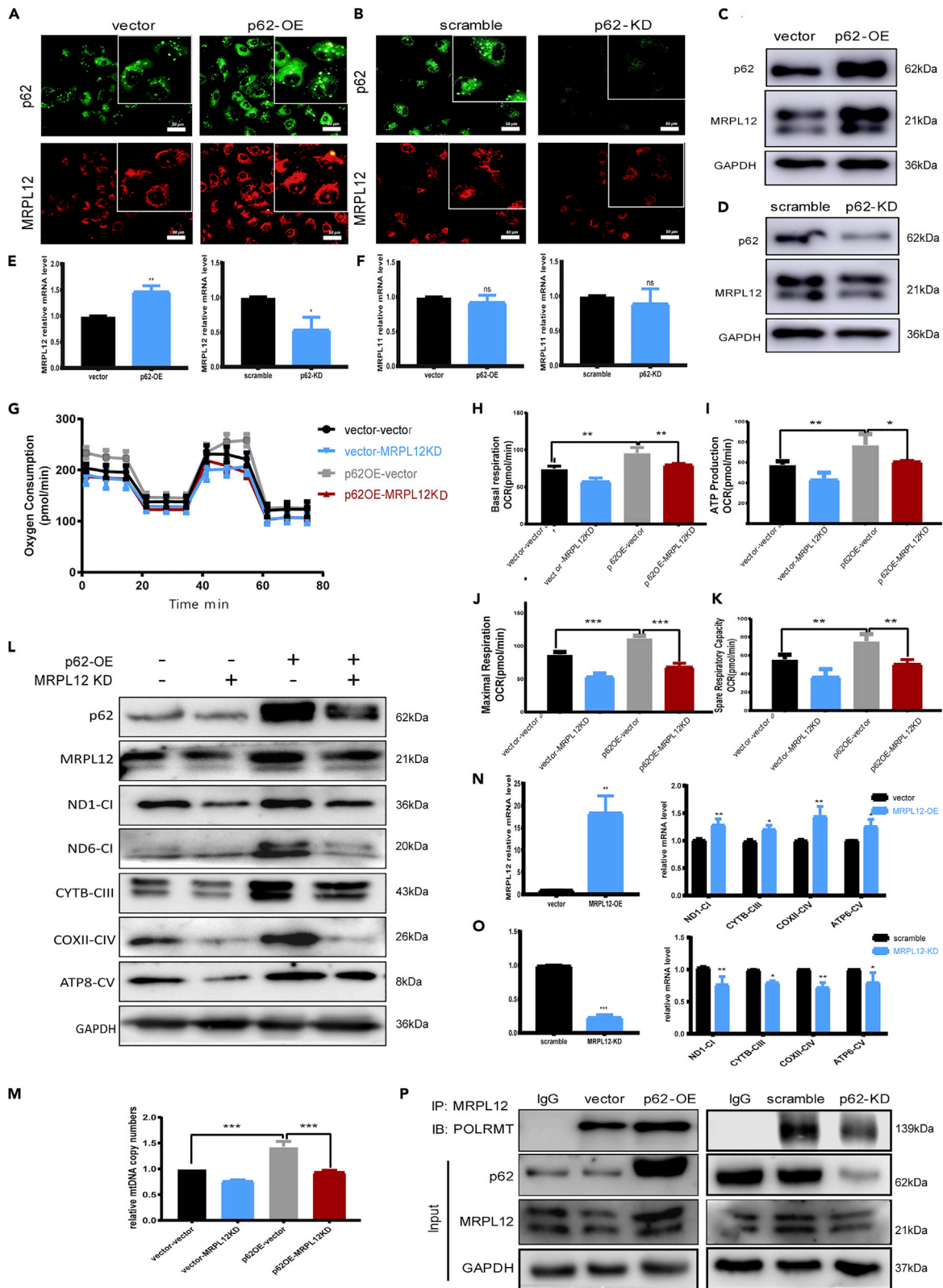
Figure 3. MRPL12 Mediates the Effects of SQSTM1/p62 on mtDNA Expression

(A–D) Expression of MRPL12 was detected on protein level by immunofluorescent staining (A and B) and western blotting (C and D) in SQSTM1/p62-overexpressed or knocked down HK-2 cells. Scale bars, 50 μm.

(E and F) mRNA levels of MRPL12 and MRPL11 detected by qRT-PCR in SQSTM1/p62-overexpressed or knocked down HK-2 cells. β-actin was used as internal control. Unpaired, two-tailed t tests were used, n = 3, *p < 0.05, **p < 0.01.

(G) Bioenergetic profiles measured by Seahorse XF96 in HK-2 cells co-transfected with SQSTM1/p62-overexpressing and MRPL12-silencing plasmids.

(H–K) Basal respiration (H), ATP production (I), maximal respiration (J), and spare respiratory capacity (K) in HK-2 cells co-transfected with SQSTM1/p62-overexpressing and MRPL12-silencing plasmids were identified, respectively. One-way ANOVA followed by Sidak's multiple comparisons test, n = 4 biological replicates, *p < 0.05, **p < 0.01, ***p < 0.001.

(L) Expression of subunits of OXPHOS complexes by western blotting in HK-2 cells co-transfected with SQSTM1/p62-overexpressing and MRPL12-silencing plasmids.

(M) mtDNA copy numbers in SQSTM1/p62-overexpressing and MRPL12-silencing duel-transfected HK-2 cells. Unpaired t tests were used, n = 3, *p < 0.05, **p < 0.01, ***p < 0.001.

(N and O) mRNA levels of ND1, CYTB, COXII, and ATP6 detected by qRT-PCR in MRPL12-overexpressed or knocked down HK-2 cells. β-actin was used as internal control. Unpaired, two-tailed t tests were used, n = 3, *p < 0.05, **p < 0.01, ***p < 0.001.

(P) Immunoblotting of POLRMT interacting with MRPL12 from SQSTM1/p62-overexpressed or knocked down HK-2 cells identified by coIP. Rabbit IgG was used as negative control.

demonstrated the *in situ* interaction of SQSTM1/p62 with p38 by proximity ligation assay (PLA) (Figures 5A and 5B), which gives a positive green signal when the two proteins of interest are within 30–40 nm. As observed by *in situ* PLA, the colocalization of SQSTM1/p62 and p38 was significantly reduced in SQSTM1/p62 silenced cells, which was also confirmed by the coIP assay that the p38 binding to SQSTM1/p62 was diminished in SQSTM1/p62 knocked down TECs (Figure 5C). Thus, we demonstrated SQSTM1/p62-induced MRPL12 expression appeared to be mediated by the p38/ATF2 signaling pathway. This conclusion was then directly evaluated by analyzing MRPLl12 expression levels in the vector or p62-OE with and without p38 knockdown (Figure 5D) and p38 activation alone (Figure 5E).

MRPL12 Is a Direct Target Gene of Transcription Factor ATF2

Then, the direct binding of ATF2 to the predicted sites within the MRPL12 promoter was evaluated as following. First, EMSA analysis demonstrated that ATF2 could indeed bind to the predicted sequence from −2,344 bp to −2,336 bp within the MRPL12 promoter (Figure 5F). Then, the binding of ATF2 was further proved by chromatin immunoprecipitation (ChIP) assay (Figure 5G), and SQSTM1/p62 plus or minus led to a significant elevation or reduction of ATF2 binding to MRPL12 (Figure 5H), suggesting SQSTM1/p62 did affect MRPL12 expression via ATF2-mediated transcription. Such conclusion was further confirmed by luciferase reporter assay. An MRPL12 promoter-driven luciferase reporter plasmid (MRPL12-Luci) and an ATF2-mutant MRPL12 promoter-driven luciferase reporter plasmid were generated, respectively (Figure 5I), and a significant elevation (2,835%) of MRPL12-Luci was evidenced (Figure 5J). Consistent with the findings of ChIP assay, SQSTM1/p62 overexpression also resulted in an additional enhancement of transcriptional activity in wild-type MRPL12-Luci transfected cells, not in mutant ones (Figure 5J). Collectively, these data evidenced that MRPL12 is a direct target gene of ATF2 and such mechanism is likely to be involved in the SQSTM1/p62-induced MRPL12 expression.

SQSTM1/p62-Mediated mtDNA Expression Participates in the Mitochondrial Response Induced by Energetic Stresses

The findings above demonstrated that SQSTM1/p62 could control mtDNA expression and OXPHOS and these effects appeared to be mediated via p38/ATF2 regulated MRPL12 transcription; then we wondered whether such mechanism participated in the mitochondrial adaptation to environmental energetic stresses, such as nutrients deprivation and hypoxia. As shown in Figures 6A and 6B, serum deprivation led to an impaired mitochondrial OXPHOS capacity, with significantly reduced basal OCR, ATP-linked OCR, maximal respiration, and spare respiratory capacity. Real-time qPCR revealed that mRNA levels of both SQSTM1/p62 and MRPL12 were also dramatically decreased under serum deprivation (Figures 6C and 6D). Concomitantly, protein levels of SQSTM1/p62, MRPL12, and mtDNA-encoded subunits of OXPHOS complexes also exhibited the same tendency (Figure 6E). Interestingly, overexpression of SQSTM1/p62 could effectively ameliorate serum deprivation-induced OXPHOS impairment (Figures 6F–6J), along with ameliorated cellular MRPL12 and OXPHOS complexes (Figure 6K) expressions.
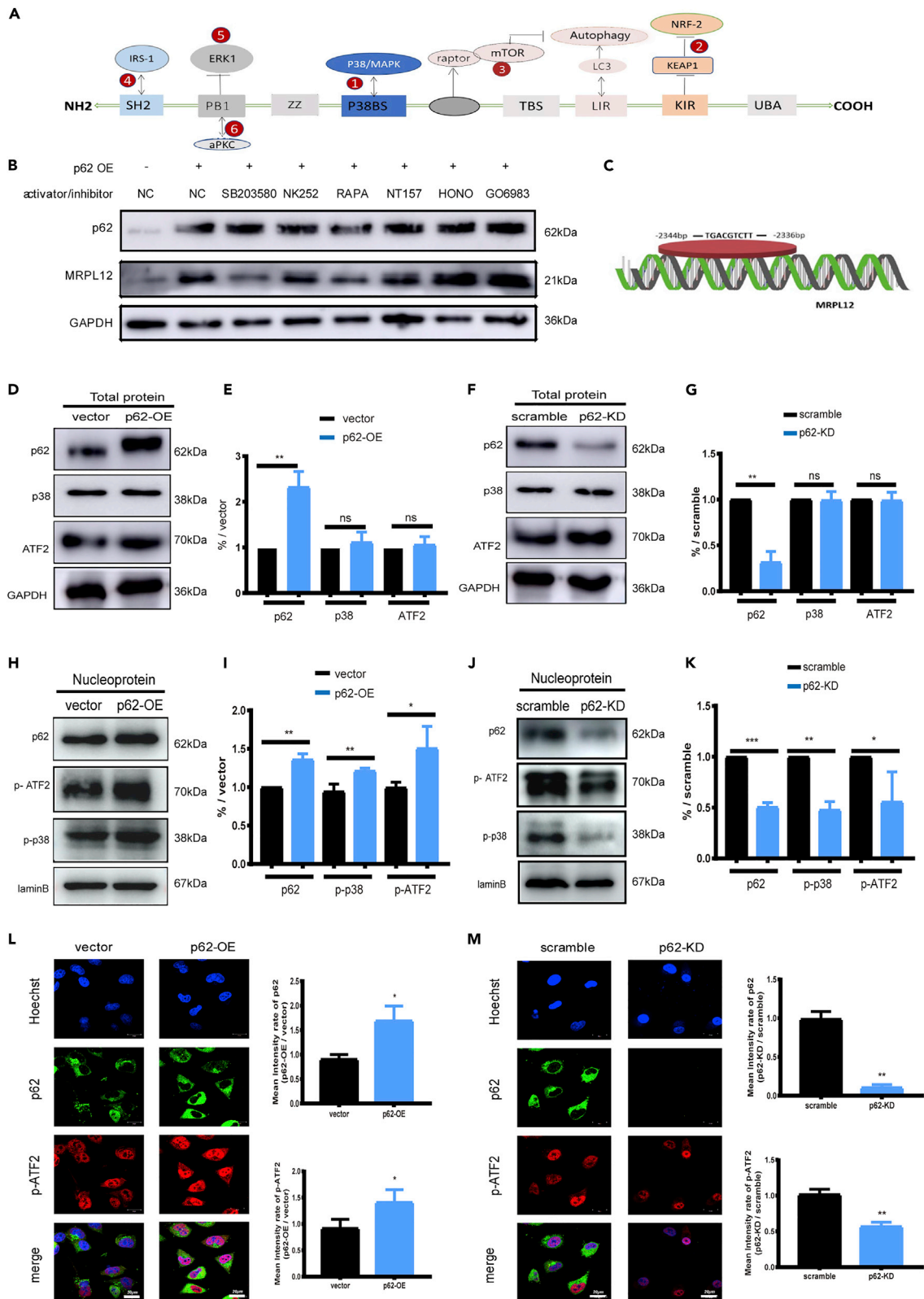
Figure 4. SQSTM1/p62 induces MRPL12 Expression via Activating p38/ATF2 Signaling Pathway

(A) Schematic diagram for SQSTM1/p62 domains and interacting partners. ① to ⑥ represent inhibitors or activators to the interacting partners as following: ① p38 inhibitor SB203580 (10 μM, Selleck); ② Nrf2 activator NK252 (20 μM, MedChemExpress); ③mTOR inhibitor rapamycin (10 μM, Selleck); ④ IRS-1/2 inhibitor NK157 (10 μM, Selleck); ⑤ ERK1/2 activator Honokiol (20 μM, Selleck); and ⑥ PKC inhibitor Go6983 (100 nM, Selleck).

(B) MRPL12 expression was detected by western blotting in SQSTM1/p62-overexpressed HK-2 cells treated with the above inhibitors or activators.

(C) A potential ATF2 binding site within the promoter region of human MRPL12 gene was identified by ALGGEN-PROMO (Version 3.0.2) between −2,344 bp and −2,336 bp upstream from the transcription start site.

(D–G) Western blotting for total p38 and ATF2 in SQSTM1/p62-overexpressed (D) or knocked down (F) HK-2 cells. GAPDH was used as internal control. (E) and (G) were grayscale analysis for (D) and (F) respectively. Unpaired t tests were used, n = 3, **p < 0.01.

(H–K) Western blotting for nuclear p-p38 and p-ATF2 in SQSTM1/p62-overexpressed (H) or knocked down (J) HK-2 cells. LaminB was used as internal control. (I) and (K) were grayscale analysis for (H) and (J) respectively. Unpaired t tests were used, n = 3, *p < 0.05, **p < 0.01, ***p < 0.001.

(L and M) Immunofluorescent staining for SQSTM1/p62 and p-ATF2 in SQSTM1/p62 transfected HK-2 cells. Nuclei were counterstained by Hoechst 33258. Scale bars, 20 μm. Mean intensity was calculated by Image Pro Plus and showed in histogram respectively. Unpaired t tests were used, n = 3, *p < 0.05, **p < 0.01.

Then, we continued to determine whether SQSTM1/p62 also had a role in hypoxia-induced mitochondrial response. The mRNA levels of both SQSTM1/p62 and MRPL12 dramatically decreased upon hypoxia treatment (Figures 6L and 6M), accompanied by diminished protein contents of SQSTM1/p62, MRPL12, and OXPHOS complexes (Figure 6N). Furthermore, SQSTM1/p62 overexpression also effectively ameliorated hypoxia-induced expressions of MRPL12 and OXPHOS complexes (Figure 6O). In general, these data above suggested that SQSTM1/p62-induced MRPL12 transcription might be a key mechanism mediating both serum deprivation and hypoxia-induced mitochondrial response in TECs.

SQSTM1/p62 Is Essential in Maintaining TECs Mitochondrial Homeostasis and Kidney Function

Based on the *in vitro* findings above, we continued to investigate whether such mechanism might also play a role in the pathogenesis of energy stress-associated diseases, such as ischemic acute kidney injury (AKI). The expression of SQSTM1/p62 and MRPL12 was evaluated in renal samples from both patients with AKI complied with the KDIGO criteria (Table S2) and mice models by immunohistochemistry. As shown in Figure 6, ischemic attack led to an obvious tubulointerstitial injury (Figures 7A and 7B), accompanied by a significant decrease of SQSTM1/p62 and MRPL12, as well as protein subunits of OXPHOS complexes in renal biopsies of patients with AKI, especially in the tubulointerstitial area (Figure 7C). Similar findings were also observed in AKI mice renal samples compared with the control littermates (Figure 7D); the mean intensity of IHC images was statistically analyzed by ImageJ (Figure S2). All the results above suggested that SQSTM1/p62 and MRPL12 are involved in the pathogenesis of AKI which may be analogous to the *in vitro* study above.

To evaluate the *in vivo* role of SQSTM1/p62 in ischemia-induced renal injuries, conditional TECs SQSTM1/p62 knockout mice (CKO) were then generated and the genotyping was first verified by PCR (Figure 8A). Immunofluorescent analysis also confirmed the specific deficiency of SQSTM1/p62 in TECs using CK18 as an epithelial marker (Figure 8B).

Unexpectedly, although no significant phenotypic alterations were observed at the age of 2 months, TECs SQSTM1/p62 CKO mice exhibited obvious kidney injuries at the age of 5 months, evidenced by oliguria, elevated serum creatinine, and BUN levels (Figures 8E–8G, and the information of the commercial assays was listed in Table S1). The body weights of CKO mice also decreased compared with their wild-type littermates at the age of 6 months (Figures 8C and 8D). Furthermore, although no obvious morphological alterations within tubulointerstitium were detected on the CKO mice by H&E staining (Figure 8H), electron microscope analysis demonstrated obvious mitochondrial injuries including irregularly arranging, mitochondrial swelling, and decreased mitochondrial abundance (Figures 8I and 8J).

Oxygen consumption determined by Clark-type oxygen electrode manifested that the mitochondrial respiration capacity was crippled in CKO mice, which was deteriorated after AKI modeling (Figure 8K). Concomitantly, immunohistochemistry study revealed that CKO mice exhibited a significant reduction of MRPL12, especially in tubulointerstitial area, as well as decreased expression of OXPHOS complexes, which were further decreased by additional loss of SQSTM1/p62 in TECs compared with AKI wild-type (WT) mice (Figure 8L), and the mean intensities were analyzed in Figure S3. These results were further confirmed by western blotting (Figure 8M).
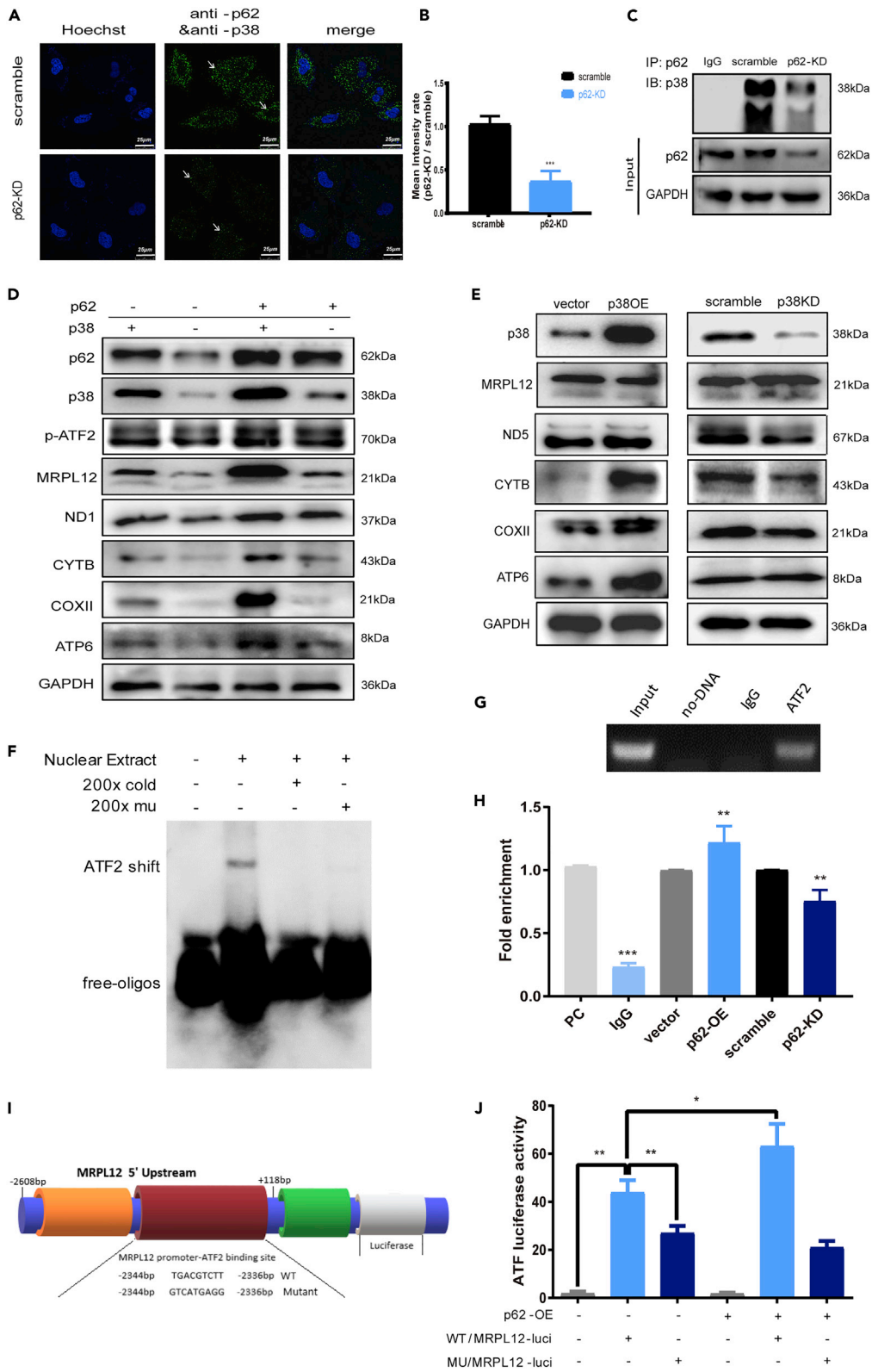
Figure 5. MRPL12 Is a Direct Target Gene of ATF2

(A and B) Interaction and quantification of SQSTM1/p62 and p38 in scramble transfected and SQSTM1/p62 knocked down HK-2 cells visualized by Duolink proximity ligation assay. The arrows indicated the interaction of SQSTM1/p. The green dots represents the interaction of SQSTM1/p62 and p38 which was also indicated by the arrows, the blue fluorescence represents the nuclei. Mean intensity was calculated by Image Pro Plus. Scale bars, 20 μm. Unpaired t tests were used, n = 3, ***p < 0.001.

(C) Co-immunoprecipitation of SQSTM1/p62 and p38 in scramble transfected and SQSTM1/p62 knocked down HK-2 cells. Mouse-IgG was used as negative control.

(D) Western blotting for p62, p38, p-ATF2, MRPL12, and OXPHOS components in SQSTM1/p62 overexpressed with or without p38 knocked down HK-2 cells.

(E) Western blotting for OXPHOS components in p38-overexpressed or knocked down HK-2 cells.

(F) The binding of ATF2 to MRPL12 promoter DNA probe in HK-2 cells nuclear extract was identified by EMSA. A cold probe and a mutant probe were used as competitors.

(G) ChIP-PCR analysis for the binding of ATF2 to MRPL12 promoter performed on HK-2 cells chromatin using rabbit anti-ATF2 antibody and rabbit IgG was used as a negative control.

(H) The occupancy of MRPL12 promoter of ATF2 was enriched by SQSTM1/p62 overexpression and deprived by SQSTM1/p62 knockdown analyzed by quantitative PCR-based ChIP assay. Unpaired t tests were used, n = 3, *p < 0.05, **p < 0.01.

(I) Schematic structure of the MRPL12 luciferase reporter. The putative ATF2 binding site-directed mutagenesis from TGACGTCTT to GTCATAGG was shown.

(J) SQSTM1/p62 overexpression significantly increased the MRPL12 luciferase reporter activity. Two-tailed with unpaired t tests were used to compare these data points, n = 3, *p < 0.05, **p < 0.01, ***p < 0.001.

Thereby, these *in vivo* findings provided further evidences supporting that SQSTM1/p62 is crucial for physiological regulation of mitochondrial OXPHOS, with p38/ATF2-mediated MRPL12 transcription and subsequent mtDNA expression as the key intermediate mechanism.

DISCUSSION

Emerging data suggest SQSTM1/p62 might have autophagy-independent effects on mitochondrial function, such as regulating BAT mitochondrial uncoupling and controlling NADH availability for electron transfer chain (Muller et al., 2013; Bartolome et al., 2017). These make SQSTM1/p62 appearing as a multifaced modulator of mitochondria, possibly owing to its multiple functional motifs (Long et al., 2017). In the present study, we further developed that SQSTM1/p62 could also act as a crucial regulator and energetic sensor of mtDNA expression machinery, and such effects were mediated by MRPL12, which was newly identified to play a part in mtDNA expression. Via activating p38/ATF2 signaling, SQSTM1/p62 could induce MRPL12 transcription and accordingly promote mtDNA expression. Furthermore, SQSTM1/p62 and MRPL12-mediated mtDNA expression is also involved in mitochondrial response to energetic challenges including nutrients deprivation and hypoxia.

Although SQSTM1/p62 was found to participate in metabolic processes and energetic homeostasis, novel downstream ligands need to be found to establish the connection of mitochondrial dysfunction and the key domain of SQSTM1/p62. As a critical component of mitochondrial ribosome, MRPL12 could also exist in a ribosome-free form within mitochondria and directly bind to POLRMT, thereby stimulating mtDNA transcription (Surovtseva et al., 2011). And the overexpression of MRPL12 was also proved to be able to modulate mitochondrial gene expression in mammalian cells (Nouws et al., 2016). Similar to our findings that SQSTM1/p62 knockdown resulted in a reduced expression of complex subunits and impaired OXPHOS rate, MRPL12 mutation also exhibited damaged complex activities, with decreased synthesis of components comprising OXPHOS complexes (Serre et al., 2013). The similar phenotypes between SQSTM1/p62 knockdown and MRPL12 mutation provide further evidences supporting our proposal that MRPL12 may be the major downstream player in SQSTM1/p62-induced mtDNA expression. Furthermore, mitochondrial DNA transcription is known to be functionally coupled to mitochondrial biogenesis, and several components comprising mtDNA transcription apparatus concomitantly act as essential players in the process of mtDNA replication, such as mitochondrial transcription factor A (TFAM) and POLRMT (Koc and Koc, 2012; Kukat et al., 2015; Hao et al., 2016). Such notion was also evidenced by our results that SQSTM1/p62-induced mtDNA expression was accompanied by elevated mitochondrial abundance (Figures 1K and 1M).

MRPL12 is the first mitochondrial ribosomal protein to be characterized in mammals (Frei et al., 2005), and its mutations lead to growth retardation, neurological deterioration, and mitochondrial translation deficiency (Serre et al., 2013). In addition, an artificial intelligence analysis showed that MRPL12 plays central roles regarding the
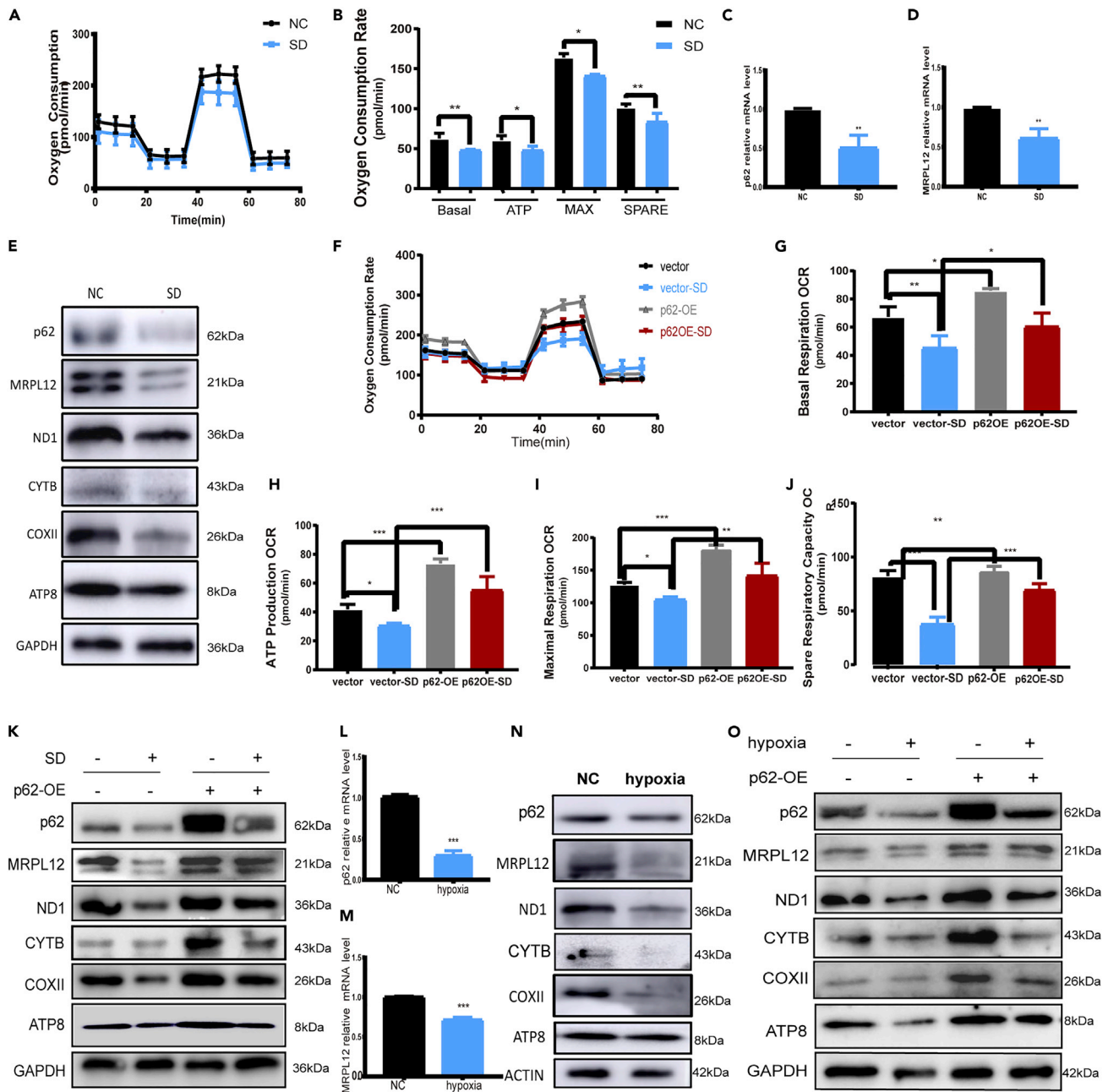
Figure 6. SQSTM1/p62-Mediated mtDNA Expression Participates in the Mitochondrial Response Induced by Energetic Stresses

(A) OCR in HK-2 cells was analyzed by Seahorse XF96 under serum deprivation (SD) for 48 h compared with normal condition (NC).

(B) Basal respiration, ATP production, maximal respiration, and spare respiratory capacity were identified, respectively. n = 4 biological replicates, one-way ANOVA followed by Sidak's multiple comparisons test, n = 4 biological replicates, *p < 0.05, **p < 0.01, ***p < 0.001.

(C and D) The mRNA levels of SQSTM1/p62 and MRPL12 were detected by qRT-PCR in HK-2 cells under 48 h serum deprivation. β-actin was used as internal control. Unpaired t tests were used, n = 3, **p < 0.01.

(E) The protein levels of SQSTM1/p62, MRPL12, and OXPHOS complexes detected by western blotting in HK-2 cells under serum deprivation.

(F–J) The amelioration of SQSTM1/p62 overexpression on serum deprivation induced OCR defects was evaluated by Seahorse XF96. The cells transfected with SQSTM1/p62 overexpression plasmid were treated by serum deprivation for 48 h. Basal respiration (G), ATP production (H), maximal respiration (I), and spare respiratory capacity (J) were identified, respectively. One-way ANOVA followed by Sidak's multiple comparisons test, n = 4 biological replicates, *p < 0.05, **p < 0.01, ***p < 0.001.

(K) Western blotting for SQSTM1/p62, MRPL12, and OXPHOS complexes in SQSTM1/p62-overexpressed cells under serum deprivation compared with controls.

effects of calorie restriction on life extension (An et al., 2008). And MRPL12 was identified as one of the significant down-regulation mitochondrial proteins in prenatal stress-related mitochondrial biogenesis in the frontal cortex and hippocampus (Olszanecki and Basta-kaim, 2015). However, the physiological regulation of MRPL12 expression is little known so far. To our knowledge, our identification of ATF2 as its transcription factor is the first report concerning MRPL12 gene expression pattern. Via binding to the promoter of MRPL12 between −2,344 bp and −2,336 bp, ATF2 could effectively induce MRPL12 transcription (Figure 5). Furthermore, the effect of ATF2 is under the control of p38 signaling and accounts for SQSTM1/p62-induced mtDNA transcription. In addition, besides controlling inflammation, immunity, and proliferation, recent studies suggested p38 might be involved in multiple metabolic processes, such as gluconeogenesis, fatty acid β-oxidation, and insulin secretion (Bordicchia et al., 2012; Jager et al., 2007; Kawai et al., 2008). Through a few important transcription factors, p38 targets several proteins with prominent roles in mitochondrial function, such as uncoupling protein 1 (UCP1) (Cao et al., 2001; Nisoli et al., 2005), thereby enhancing mitochondrial OXPHOS and mtDNA expression. Our results established MRPL12 as a new downstream effector p38, thus mediating its effects on mitochondrial dysfunction in metabolic diseases.

It should be mentioned that, besides ATF2, several other transcription factors including NFE2L2/Nrf2 (nuclear factor, erythroid 2-like 2) and NF-κB (nuclear factor kappa B) were also predicted to be capable of binding to the MRPL12 promoter and might activate its transcription (data available on request). We did not explore these factors because among the main SQSTM1/p62-interacting signaling pathways, only p38 and mTOR signaling were evidenced to be involved in SQSTM1/p62's induction of MRPL12 expression (Figure 4B) (Kawai et al., 2008), whereas ATF2 is a known downstream effector of p38 signaling (Dodson et al., 2013). However, whether NFE2L2/Nrf2 and NF-κB might also act as potential transcription factors of MRPL12 is another interesting topic deserving future identification, as both molecules are known to be involved in ample cellular processes such as inflammation, stress response, and tumorigenesis (Bartolini et al., 2018; Mitchell et al., 2016).

When challenged by nutrient crises such as ischemia and hypoxia, cells are known to switch its energy production from mitochondrial OXPHOS to anaerobic glycolysis (Ham and Raju, 2017; Haran and Gross, 2014). Such effects could be achieved by concurrent upregulated synthesis of glycolysis enzymes and downregulated expression of OXPHOS components. This metabolic reprogramming is of significance in cell survival during the early phase of energy stresses, whereas persistent inhibition of OXPHOS might induce oxidative stress and cell apoptosis (Vempati et al., 2008; Mejlvang et al., 2018; Jiang et al., 2010). Several signaling pathways are known to be involved in this process, such as hypoxia-inducible factor 1α (HIF-1α) signaling and AMPK pathway (Palm and Thompson, 2017; Yamamoto et al., 2016). Our present study indicated that SQSTM1/p62-induced MRPL12 transcription might be another mechanism underlying. Both serum deprivation and hypoxia resulted in a significant decline of SQSTM1/p62 content along with concomitant impairments of p38 signaling, MRPL12 level, mtDNA expression, and OXPHOS activity, whereas replenishment of SQSTM1/p62 effectively ameliorated such abnormalities (Figure 5). Furthermore, energy stresses are known to induce the degradation of SQSTM1/p62 by inspiring autophagic flux (Kaushal and Shah, 2016; Zhou et al., 2018). Although the role of autophagic degradation could not be excluded, the decreased mRNA level of SQSTM1/p62 indicated that a transcriptional adapting mechanism of SQSTM1/p62 might exist as well (Figures 6C and 6L). It seems that SQSTM1/p62 might act as an active player participating in energy crises associated bioenergetic reprogramming, not only as a simple passive mediator secondary to the autophagic flux.

An unexpected finding of the present study is that TECs-specific SQSTM1/p62 knockout mice exhibited obvious kidney injury, characterized by oliguria and increased serum creatinine and BUN levels (Figures 8E–8G). Such results suggested that SQSTM1/p62 plays a key role in maintaining TECs homeostasis. As shown by Müller and colleagues, adipocyte-specific SQSTM1/p62 deficiency led to a significant impairment of BAT thermogenesis, whereas SQSTM1/p62 deficiency in liver or muscle had no obvious effects on the function of these organs (Muller et al., 2013). Taking all these findings into account, SQSTM1/p62 seems to be essential for those cell types in which cellular homeostasis heavily relies on mitochondria. Such proposal also coincides with the emerging role of SQSTM1/p62 in mitochondrial regulation. As to
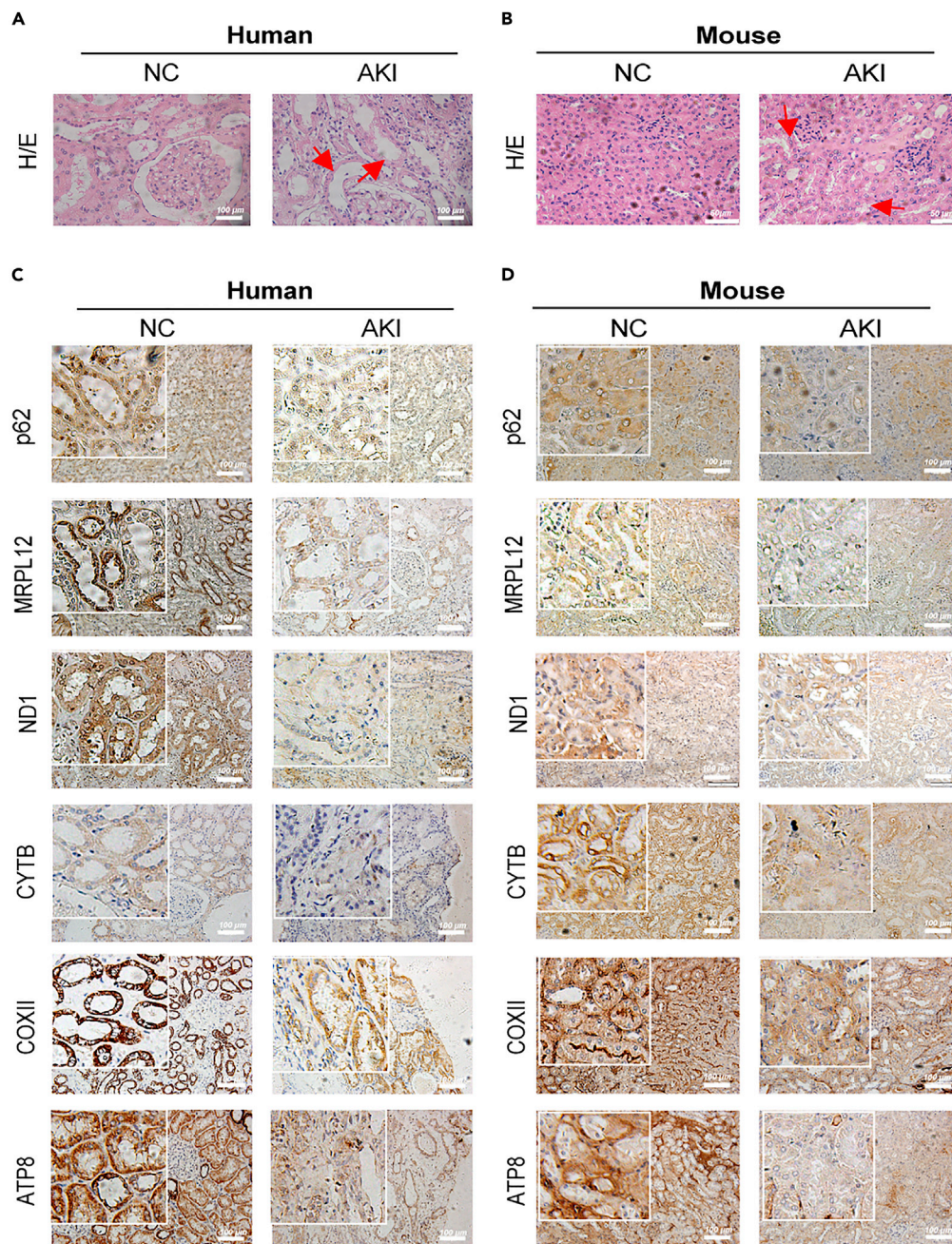
Figure 7. Tubulointerstitial Injuries in Both Patients with AKI and Mouse Model

(A and B) H&E staining for patients (A) and mice (B) with AKI compared with controls, with arrows indicating the tubulointerstitial injuries. Scale bars, 50 or 100 μm.

(C and D) Immunohistochemistry staining for SQSTM1/p62, MRPL12, and OXPHOS complexes (ND1, CYTB, COXII and ATP8) detected in patients (C) and mice (D) with AKI. Scale bars, 100 μm.

be mentioned, TECs-specific SQSTM1/p62 knockout mice exhibited mildly decreased body weights (Figure 8D) in contrast to the results observed in SQSTM1/p62 global-knockout mice (Muller et al., 2013). Such inconsistence might be due to the systemic metabolic disturbance induced by SQSTM1/p62 depletion as both obesity and diabetic states exhibited in SQSTM1/p62 global-knockout mice are known to be capable of inducing kidney hypertrophy. Finally, our identification that SQSTM1/p62 plays an essential role in TECs
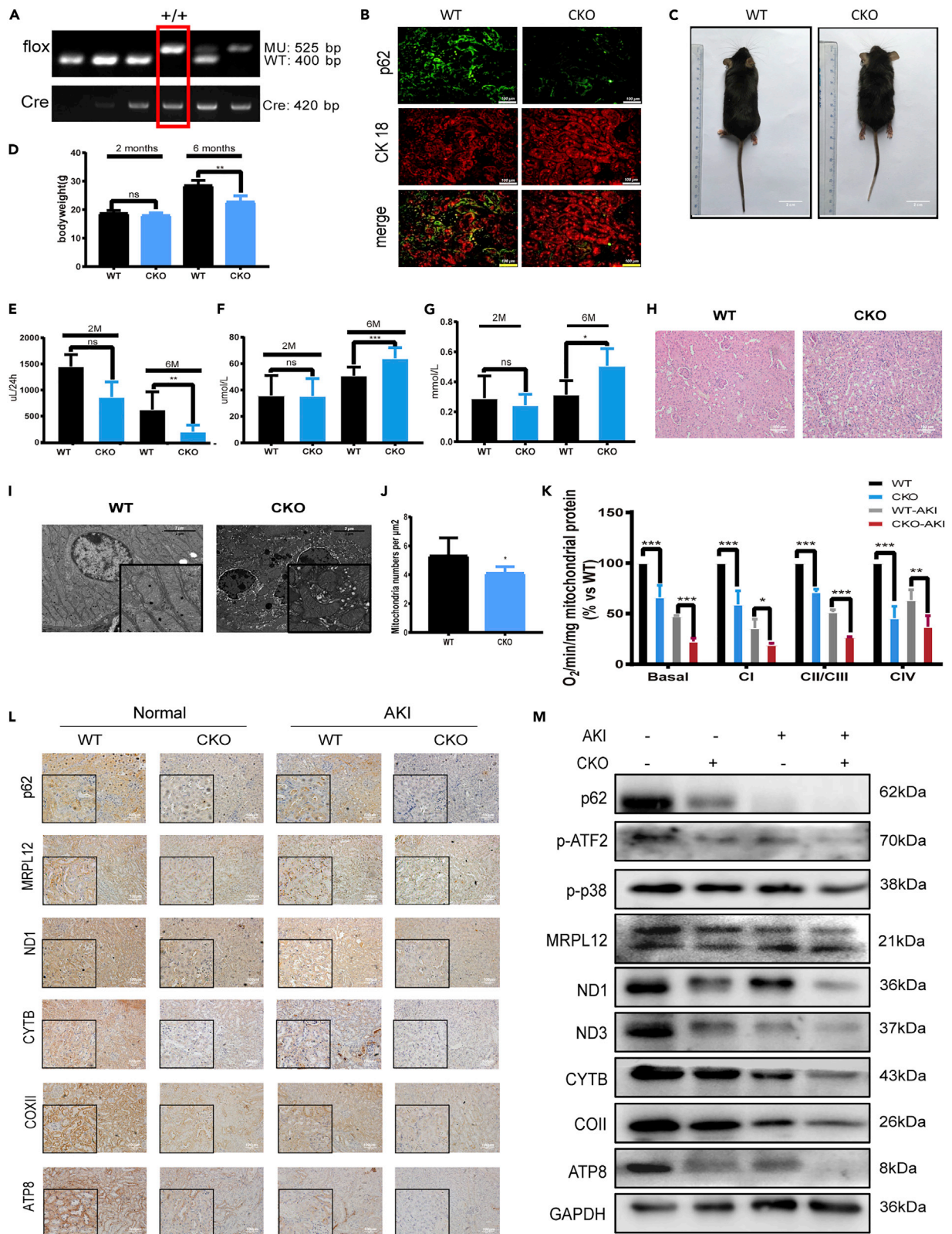
Figure 8. TECs-Specific SQSTM1/p62 Knockout Mice Exhibited Kidney Injuries

(A) Genotyping of TECs-specific SQSTM1/p62 knockout mice. +/+ indicates homozygote.

(B) Immunofluorescent staining confirmed the deficiency of SQSTM1/p62 in renal epithelial tubules with CK18 as a marker. Scale bars, 100 μm.

(C) The morphology of SQSTM1/p62 TECs CKO mice and their kidneys at the age of 6 months compared with wild-type littermates.

(D) The body weights of SQSTM1/p62 CKO mice at the age of 2 and 6 months compared with wild-type littermates. n = 5, *p < 0.05.

(E–G) Urine volume (E), serum creatinine (F), and BUN (G) were measured in WT and CKO mice at the age of 2 and 6 months. Unpaired t tests were used, *p < 0.05, **p < 0.01, ***p < 0.001.

(H) H&E staining for WT and SQSTM1/p62 CKO mice. Scale bars, 100 μm.

(I) Electron microscopy analysis for TECs mitochondria in renal samples of WT and SQSTM1/p62 CKO mice. Scale bars, 2 μm.

(J) Mitochondria numbers per μm^2 of (J) were counted using Image-Pro Plus 6.0. Unpaired t tests were used, n = 6, *p < 0.05.

(K) Oxygen consumption was recorded by Clark-type electrode in WT and SQSTM1/p62 CKO mice under normal or AKI treatments after the addition of substrates and inhibitors for Complex I (5 mM Glutamate plus 5 mM Malate and 2 mM Rotenone), Complex II + III (5 mM Succinate plus 5 mM Glyceraldehyde-3-P and 0.1 mM Antimycin), and Complex IV (1.2 mM TMPD and 6 mM KCN). n = 3, *p < 0.05, **p < 0.01, ***p < 0.001.

(L) Immunohistochemistry staining for p62, MRPL12, and subunits of OXPHOS complexes in renal samples of WT and SQSTM1/p62 CKO mice under normal or AKI treatments. Scale bars, 100 μm.

(M) Western blotting for p62, MRPL12, and OXPHOS complexes in renal samples of WT and SQSTM1/p62 CKO mice under normal or AKI treatments.

homeostasis suggested SQSTM1/p62 might be a potential target in intervening ischemic or hypoxic kidney injury. Although *in vivo* evidences employing SQSTM1/p62-overexpressing animals are lacking currently, our *in vitro* SQSTM1/p62-overexpressing studies in TECs (Figure 6), as well as several others' studies demonstrated that inhibiting autophagy, which could lead to cellular SQSTM1/p62 accumulation, all indicated that SQSTM1/p62 have protective effects on ischemic kidney injuries (Yamamoto et al., 2016; Kaushal and Shah, 2016).

In conclusion, our study suggested SQSTM1/p62 could act as a crucial modulator and energy sensor of mtDNA transcription and the effects are mediated by p38-ATF2 signaling-dependent MRPL12 expression.

Limitations of the Study

One limitation of the study is the lack of conditional TECs SQSTM1/p62 knockin mice. It remains to be seen if the increase in SQSTM1/p62 expression in the renal TECs elevates the OXPHOS in TECs and ameliorates the symptoms of AKI.

Another limitation of the study is that the effect of MRPL12 levels on mitochondrial gene expression via POLRMT has previously already been observed and we propose a direct signaling pathway back to p62.However, although we demonstrate that ATF2 can interact with a promoter region in the MRPL12 locus, it is not clear in what way this interaction affects MRPL12 gene expression and further experiments are needed to address the detailed mechanism.

RESOURCE AVAILABILITY

Lead Contact

Further information and requests for resources and reagents should be directed to and will be fulfilled by the Lead Contact, Qiang Wan (wanqiang@sdu.edu.cn).

Materials Availability

This study did not generate new unique reagents.

Data and Code Availability

Original samples, data, and transduced cells are available upon request.

Ethical Approval

All human samples obtained from human subjects were approved by the institutional review board of Cheeloo College of Medicine, Shandong University (ECSBMSSDU2018-1-045), and written informed consent was provided prior to enrollment into the study. All experiments were approved by institutional animal care and use committee of Shandong University.

METHODS

All methods can be found in the accompanying Transparent Methods supplemental file.

REFERENCES

An, L., Approach, A.I., Goertzel, B., Pennachin, C., Mudado, M.D.A., and Coelho, L.D.S. (2008). Identifying the genes and genetic interrelationships underlying the impact of calorie restriction on maximum. Rejuvenation Res. *11*, 735–748.

Andrea, A.D., Gritti, I., Nicoli, P., Giorgio, M., Doni, M., Conti, A., Bianchi, V., Casoli, L., Sabò, A., Alexandre, M., et al. (2016). The mitochondrial translation machinery as a therapeutic target in Myc-driven lymphomas. Oncotarget *5*, 72415–72430.

Barshad, G., Blumberg, A., Cohen, T., and Mishmar, D. (2018a). Human primitive brain displays negative mitochondrial-nuclear expression correlation of respiratory genes. Genome Res. *28*, 952–967.

Barshad, G., Blumberg, A., Cohen, T., and Mishmar, D. (2018b). Mitochondrial DNA transcription and its regulation: an evolutionary perspective. Trends Genet. *34*, 682–692.

Bartolini, D., Dallaglio, K., Torquato, P., Piroddi, M., and Galli, F. (2018). Nrf2-p62 autophagy pathway and its response to oxidative stress in hepatocellular carcinoma. Transl Res. *193*, 54–71.

Bartolome, F., Esteras, N., Martin-Requero, A., Boutoleau-Bretonniere, C., Vercelletto, M., Gabelle, A., Le Ber, I., Honda, T., Dinkova-Kostova, A.T., Hardy, J., et al. (2017). Pathogenic p62/SQSTM1 mutations impair energy metabolism through limitation of mitochondrial substrates. Sci. Rep. *7*, 1666.

Bhargava, P., and Schnellmann, R.G. (2017). Mitochondrial energetics in the kidney. Nat. Rev. Nephrol. *13*, 629–646.

Blacker, T.S., and Duchen, M.R. (2016). Investigating mitochondrial redox state using NADH and NADPH autofluorescence. Free Radic. Biol. Med. *100*, 53–65.

Bordicchia, M., Liu, D., Amri, E.Z., Ailhaud, G., Dessì-Fulgheri, P., Zhang, C., Takahashi, N., Sarzani, R., and Collins, S. (2012). Cardiac natriuretic peptides act via p38 MAPK to induce the brown fat thermogenic program in mouse and human adipocytes. J. Clin. Invest. *122*, 1022–1036.

Calvo-Garrido, J., Maffezzini, C., Schober, F.A., Clemente, P., Uhlin, E., Kele, M., Stranneheim, H., Lesko, N., Bruhn, H., Svenningsson, P., et al. (2019). SQSTM1/p62-Directed metabolic reprogramming is essential for normal neurodifferentiation. Stem Cell Reports *12*, 696–711.

Cao, W., Medvedev, A.V., Daniel, K.W., and Collins, S. (2001). beta-Adrenergic activation of p38 MAP kinase in adipocytes: cAMP induction of the uncoupling protein 1(UCP1) gene requires p38 MAP kinase. J. Biol. Chem. *276*, 27077–27082.

Cavdar Koc, E., Ranasinghe, A., Burkhart, W., Blackburn, K., Koc, H., Moseley, A., and Spremulli, L.L. (2001). A new face on apoptosis: death-associated protein 3 and PDCD9 are mitochondrial ri- bosomal proteins. FEBS Lett. *492*, 166–170.

Cheng, Z., and Ristow, M. (2013). Mitochondria and metabolic homeostasis. Antioxid. Redox Signal. *19*, 240–242.

Dodson, M., Darley-Usmar, V., and Zhang, J. (2013). Cellular metabolic and autophagic pathways: traffic control by redox signaling. Free Radic. Biol. Med. *63*, 207–221.

Frei, C., Galloni, M., Hafen, E., and Edgar, B.A. (2005). The Drosophila mitochondrial ribosomal protein mRpL12 is required for Cyclin D/Cdk4-driven growth. EMBO J. *24*, 623–634.

Gustafsson, C.M., Falkenberg, M., and Larsson, N.G. (2016). Maintenance and expression of mammalian mitochondrial DNA. Annu. Rev. Biochem. *85*, 133–160.

Ham, P.B., and Raju, R. (2017). Mitochondrial function in hypoxic ischemic injury and influence of aging. Prog. Neurobiol. *157*, 92–116.

Hao, X.D., Chen, Z.L., Qu, M.L., Zhao, X.W., Li, S.X., and Chen, P. (2016). Decreased integrity, content, and increased transcript level of mitochondrial DNA are associated with Keratoconus. PLoS One *11*, e0165580.

Haran, M., and Gross, A. (2014). Balancing glycolysis and mitochondrial OXPHOS: lessons from the hematopoietic system and exercising muscles. Mitochondrion *19*, 3–7.

Hisatsune, J., Nakayama, M., Isomoto, H., Kurazono, H., Mukaida, N., Asish, K., Mukhopadhyay, Azuma, T., Yamaoka, Y., Jan, S., et al. (2008). Molecular characterization of Helicobacter pylori VacA induction of IL-8 in U937 cells reveals a prominent role for p38 MAPK in activating transcription factor-2, cAMP response element binding protein, and NF-kappaB activation. J. Immunol. *180*, 5017–5027.

Huang, J., Duran, A., Reina-Campos, M., Valencia, T., Castilla, E.A., Muller, T.D., Tschop, M.H., Moscat, J., and Diaz-Meco, M.T. (2018). Adipocyte p62/SQSTM1 suppresses tumorigenesis through opposite regulations of metabolism in adipose tissue and tumor. Cancer Cell *33*, 770–784.e6.

Jager, S., Handschin, C., St-Pierre, J., and Spiegelman, B.M. (2007). AMP-activated protein kinase (AMPK) action in skeletal muscle via direct phosphorylation of PGC-1alpha. Proc. Natl. Acad. Sci. U S A *104*, 12017–12022.

Jiang, M., Liu, K., Luo, J., and Dong, Z. (2010). Autophagy is a renoprotective mechanism during in vitro hypoxia and in vivo ischemia-reperfusion injury. Am. J. Pathol. *176*, 1181–1192.

Kanayama, M., Inoue, M., Danzaki, K., Hammer, G., He, Y.W., and Shinohara, M.L. (2015). Autophagy enhances NFkappaB activity in specific tissue macrophages by sequestering A20 to boost antifungal immunity. Nat. Commun. *6*, 5779.

Kashuba, E., Yurchenko, M., Yenamandra, S.P., Snopok, B., Isaguliants, M., Szekely, L., and Klein, G. (2008). EBV-encoded EBNA-6 binds and targets MRS18-2 to the nucleus, resulting in the disruption of pRb-E2F1 complexes. Proc. Natl. Acad. Sci. U S A *105*, 5489–5494.

Kaushal, G.P., and Shah, S.V. (2016). Autophagy in acute kidney injury. Kidney Int. *89*, 779–791.

Kawai, K., Saito, A., Sudo, T., and Osada, H. (2008). Specific regulation of cytokine-dependent p38 MAP kinase activation by p62/SQSTM1. J. Biochem. *143*, 765–772.

Koc, E.C., and Koc, H. (2012). Regulation of mammalian mitochondrial translation by post-translational modifications. Biochim. Biophys. Acta *1819*, 1055–1066.

Kukat, C., Davies, K.M., Wurmd, C.A., Spåhra, H., Bonekampa, N.A., Kühla, I., Joos, F., Polosa, P.L., Park, C.B., Posse, V., and Falkenberg, M. (2015). Cross-strand binding of TFAM to a single mtDNA molecule forms the mitochondrial nucleoid. Proc. Natl. Acad. Sci. U S A *112*, 11288–11293.

Lamark, T., Svenning, S., and Johansen, T. (2017). Regulation of selective autophagy: the p62/SQSTM1 paradigm. Essays Biochem. *61*, 609–624.

Lee, S.J., Pfluger, P.T., Kim, J.Y., Nogueiras, R., Duran, A., Pagès, G., Pouysségur, J., Tschöp, M.H., Diaz-Meco, M.T., and Moscat, J. (2010). A functional role for the p62-ERK1 axis in the control of energy homeostasis and adipogen- esis. EMBO Rep. *11*, 226–232.

Long, M., Li, X., Li, L., Dodson, M., Zhang, D., and Zheng, H. (2017). Multifunctional p62 effects underlie diverse metabolic diseases. Trends Endocrinol. Metab. *28*, 818–830.

Macao, B., Uhler, J.P., Siibak, T., Zhu, X., Shi, Y., Sheng, W., Olsson, M., Stewart, J.B., Gustafsson, C.M., Falkenberg, M., et al. (2015). The exonuclease activity of DNA polymerase g is required for ligation during mitochondrial DNA replication. Nat. Commun *6*, 7303.

Mejlvang, J., Olsvik, H., Svenning, S., Bruun, J.A., Abudu, Y.P., Larsen, K.B., Brech, A., Hansen, T.E., Brenne, H., Hansen, T., et al. (2018). Starvation induces rapid degradation of selective autophagy receptors by endosomal microautophagy. J. Cell Biol. *217*, 3640–3655.

Mitchell, S., Vargas, J., and Hoffmann, A. (2016). Signaling via the NFkappaB system. Wiley Interdiscip. Rev. Syst. Biol. Med. *8*, 227–241.

Muller, T.D., Lee, S.J., Jastroch, M., Kabra, D., Stemmer, K., Aichler, M., Abplanalp, B., Ananthakrishnan, G., Bhardwaj, N., Collins, S., et al. (2013). p62 Links β-adrenergic input to mitochondrial function and thermogenesis. J. Clin. Invest. *123*, 469–478.

Nisoli, E., Tonello, C., Cardile, A., Cozzi, V., Bracale, R., Tedesco, L., Falcone, S., Valerio, A., Cantoni, O., Clementi, E., et al. (2005). Calorie restriction promotes mitochondrial biogenesis by inducing the expression of eNOS. Science *310*, 314–317.

Nouws, J., Goswami, A.V., Bestwick, M., McCann, B.J., Surovtseva, Y.V., and Shadel, G.S. (2016). Mitochondrial ribosomal protein L12 is required for POLRMT stability and exists as two forms generated by alternative proteolysis during import. J. Biol. Chem. *291*, 989–997.

Nunnari, J., and Suomalainen, A. (2012). Mitochondria: in sickness and in health. Cell *148*, 1145–1159.

Olszanecki, R., and Basta-kaim, A. (2015). Maternal stress predicts altered biogenesis and the profile of mitochondrial proteins in the frontal cortex and hippocampus of adult offspring rats. Psychoneuroendocrinology *60*, 151–162.

Palm, W., and Thompson, C.B. (2017). Nutrient acquisition strategies of mammalian cells. Nature *546*, 234–242.

Reilly, S.M., Ahmadian, M., Zamarron, B.F., Chang, L., Uhm, M., Poirier, B., Peng, X., Krause, D.M., Korytnaya, E., Neidert, A., et al. (2015). A subcutaneous adipose tissue-liver signalling axis controls hepatic gluconeogenesis. Nat. Commun. *6*, 6047.

Rodriguez, A., Duran, A., Selloum, M., Champy, M.F., Diez-Guerra, F.J., Flores, J.M., Serrano, M., Auwerx, J., Diaz-Meco, M.T., Moscat, J., et al. (2006). Mature-onset obesity and insulin resistance in mice deficient in the signaling adapter p62. Cell Metab. *3*, 211–222.

Saito, A., Kawai, K., Takayama, H., Sudo, T., and Osada, H. (2008). Improvement of photoaffinity SPR imaging plat- form and determination of the binding site of p62/SQSTM1 to p38 MAP kinase. Chem. Asian J. *3*, 1607–1612.

Satoh, J., Kawana, N., and Yamamoto, Y. (2013). Pathway analysis of ChIP-seq-based NRF1 target genes suggests a logical hypothesis of their involvement in the pathogenesis of neurodegenerative diseases. Gene Regul. Syst. Biol. *7*, 139–152.

Scarpulla, R.C. (2008). Nuclear control of respiratory chain expression by nuclear respiratory factors and PGC-1-related coactivator. Ann. N. Y Acad. Sci. *1147*, 321–334.

Seibenhener, M.L., Du, Y., Diaz-Meco, M.T., Moscat, J., Wooten, M.C., and Wooten, M.W. (2013). A role for sequestosome 1/p62 in mitochondrial dynamics, import and genome integrity. Biochim. Biophys. Acta *1833*, 452–459.

Serre, V., Rozanska, A., Beinat, M., Chretien, D., Boddaert, N., Munnich, A., Rotig, A., and Chrzanowska-Lightowlers, Z.M. (2013). Mutations in mitochondrial ribosomal protein MRPL12 leads to growth retardation, neurological deterioration and mitochondrial translation deficiency. Biochim. Biophys. Acta *1832*, 1304–1312.

Sharma, M.R., Koc, E.C., Datta, P.P., Booth, T.M., Spremulli, L.L., and Agrawal, R.K. (2003). Structure of the mammalian mitochondrial ribosome reveals an expanded functional role for its component proteins. Cell *115*, 97–108.

Sudo, T., Maruyama, M., and Osad, H. (2000). p62 functions as a p38 MAP kinase regulator. Biochembiophys Res. Commun. *269*, 521–525.

Surovtseva, Y.V., Shutt, T.E., Cotney, J., Cimen, H., Chen, S.Y., Koc, E.C., and Shadel, G.S. (2011). Mitochondrial ribosomal protein L12 selectively associates with human mitochondrial RNA polymerase to activate transcription. Proc. Natl. Acad. Sci. U S A *108*, 17921–17926.

Vempati, U.D., Torraco, A., and Moraes, C.T. (2008). Mouse models of oxidative phosphorylation dysfunction and disease. Methods *46*, 241–247.

Yamamoto, T., Takabatake, Y., Kimura, T., Takahashi, A., Namba, T., Matsuda, J., Minami, S., Kaimori, J.Y., Matsui, I., Kitamura, H., et al. (2016). Time-dependent dysregulation of autophagy: implications in aging and mitochondrial homeostasis in the kidney proximal tubule. Autophagy *12*, 801–813.

Yang, Y., Willis, T.L., Button, R.W., Strang, C.J., Fu, Y., Wen, X., Grayson, P.R.C., Evans, T., Sipthorpe, R.J., Roberts, S.L., et al. (2019). Cytoplasmic DAXX drives SQSTM1/p62 phase condensation to activate Nrf2-mediated stress response. Nat. Commun. *10*, 3759.

Zhang, X.L., Wang, Z.Z., Shao, Q.H., Zhang, Z., Li, L., Guo, Z.Y., Sun, H.M., Zhang, Y., and Chen, N.H. (2019). RNAi-mediated knockdown of DJ-1 leads to mitochondrial dysfunction via Akt/GSK-3ss and JNK signaling pathways in dopaminergic neuron-like cells. Brain Res. Bull. *146*, 228–236.

Zhou, J., Fan, Y., Zhong, J., Huang, Z., Huang, T., Lin, S., and Chen, H. (2018). TAK1 mediates excessive autophagy via p38 and ERK in cisplatin-induced acute kidney injury. J. Cell Mol Med. *22*, 2908–2921.

Supplemental Information

SQSTM1/p62 Controls mtDNA Expression

and Participates in Mitochondrial

Energetic Adaption via MRPL12

Yuan Ma, Suwei Zhu, Tingting Lv, Xia Gu, Hong Feng, Junhui Zhen, Wei Xin, and Qiang Wan
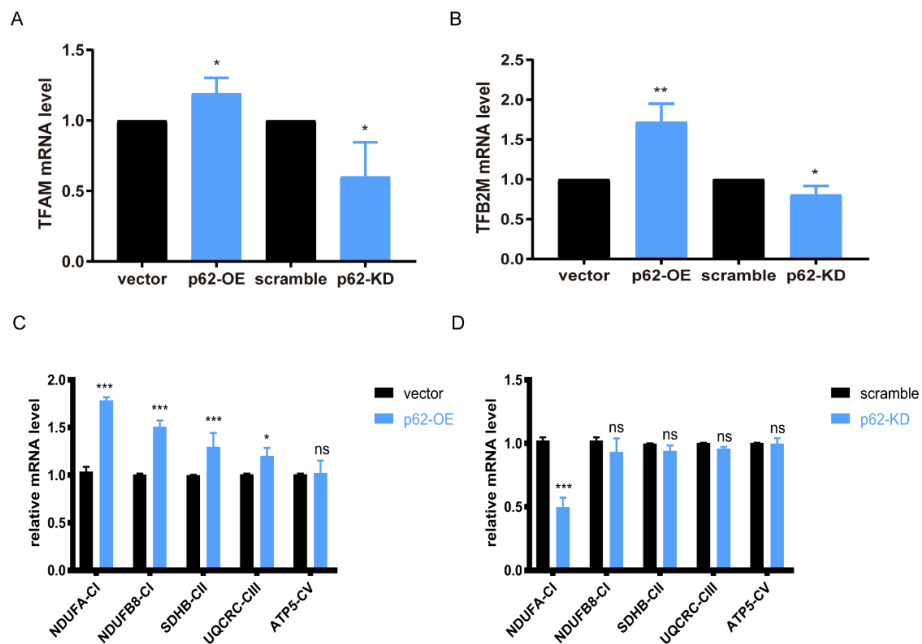
Figure S1 (Related to Figure 1)

Figure S1: The mRNA levels of nDNA-encoded genes related to mitochondrial OXPHOS. Related to Figure 1.

Figure S1A: The mRNA levels of TFAM and TFB2M were detected by qRT-PCR in SQSTM1/p62 overexpressed or knocked down HK-2 cells. Unpaired *t*-tests were used, n=3, *P<0.05, **P<0.01.

Figure S1B: The mRNA levels of nuclear encoded genes were detected by qRT-PCR in SQSTM1/p62 overexpressed or knocked down HK-2 cells. Unpaired *t*-tests were used, n=3, *P<0.05, **P<0.01.

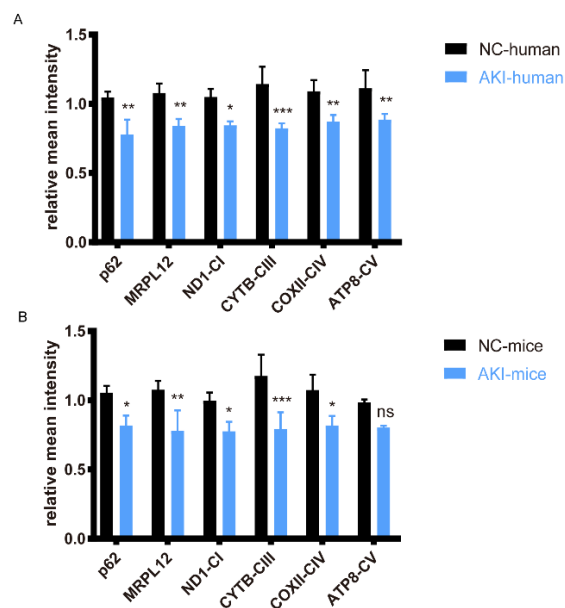**Figure S2** (Related to Figure 7)

Figure S2: The mean intensity of immunohistochemistry staining in AKI patients and mice. Related

to Figure 7.

Figure S2A and S2B: The mean intensity of immunohistochemistry staining for SQSTM1/p62, MRPL12 and OXPHOS complexes detected in AKI patients and mice were calculated by Image J, Unpaired t-tests were used, n=3, *P<0.05.
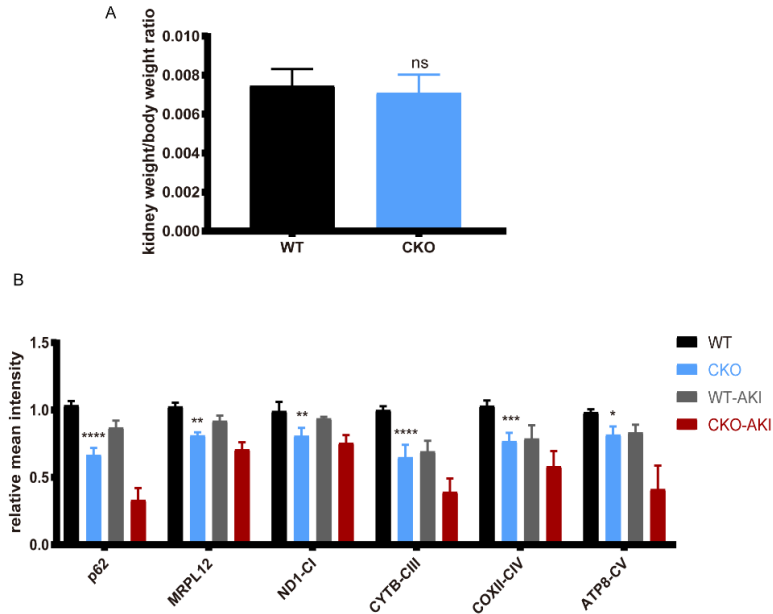
Figure S3 (Related to Figure 8)

Figure S3: The ratio of weight and the mean intensities of related genes in CKO mice and WT mice. Related to Figure 8.

Figure S3A: The ratio of kidney weight and body weight in CKO mice and WT mice. Unpaired t-tests were used, n=5, ns>0.05.

Figure S3B: The mean intensity of immunohistochemistry staining for SQSTM1/p62, MRPL12 and OXPHOS complexes detected in CKO and WT mice with or without AKI were calculated by Image J, Unpaired t-tests were used, n=3, *P<0.05.

Supplemental Tables

Table S2: The KDIGO criteria (Related to Figure 7)

Stage of AKI	Serum Creatinine	Urine output
1	1.5 - 1.9 times baseline; ≥0.3 mg/dl (≥26.5 μmol/l) increase within 48 h	<0.5 ml/kg/h for 6 - 12 h
2	2.0 - 2.9 times baseline	<0.5 ml/kg/h for ≥12 h
3	≥3.0 times baseline; Increase in serum creatinine to ≥4.0 mg/dl (≥353.6 μmol/l); Initiation of renal replacement therapy	<0.3 ml/kg/h for ≥24 h; Anuria for ≥12 h

Transparent Methods

Human subjects

Tissue sections from formalin-fixed paraffin-embedded renal biopsies from male patients with diagnosis of AKI were obtained from Cheeloo College of Medicine, Shandong University. All human samples obtained from human subjects were approved by the institutional review board of Cheeloo College of Medicine, Shandong University (ECSBMSSDU2018-1-045), and written informed consent were provided prior to enrollment into the study.

The inclusion criteria for patients with acute renal injury

All patients met the KDIGO criteria for diagnosis of ischemic AKI in adults. n=5. The KDIGO criteria was involved in Table S2.

Mouse models

Eight- to twenty-week-old male C57BL/6J mice were used in this study. Mice were housed in temperature- and humidity-controlled environments and kept on a 12:12h day/night cycle with access to standard mouse chow and water ad libitum. All experiments were approved by institutional animal care and use committee of Shandong University. Ksp1.3-Cre transgenic mice were purchased from the Jackson Laboratories (012237). SQSTM1/p62$^{fl/fl}$ mice, which harbor loxP sites flanking exon 1 of SQSTM1/p62, were generated by Shanghai Model Organisms Center, Inc. SQSTM1/p62$^{fl/fl}$ mice were bred with Ksp1.3-Cre mice to generate mice with a deletion of SQSTM1/p62 in the renal tubular epithelial cells. All experiments were performed with littermate controls. Acute kidney injury was induced by unilateral renal artery clamping plus contralateral nephrectomy as described (Yang et al, 2018). Mice were killed at 48h after reperfusion, and the kidneys, blood, and urine were collected for further analysis.

Human renal tubular epithelial cell line

Human renal proximal tubular epithelial cells (HK-2) were obtained from the American Type Culture Collection (ATCC, Manassas, VA). Cells were cultured in DMEM medium (Gibco™, Grand Island, NY) supplemented with 10 % fetal bovine serum (FBS, Gibco® Grand Island, NY), penicillin (100 U / ml) and streptomycin (100 mg / ml; Thermo Fisher Scientific) in a humidified atmosphere of 5 % (v/v) CO_2 in air at 37℃. For ischemic treatment, the cells were cultured in DMEM without serum at 37℃ for 48h, and for hypoxia treatment, cells were incubated in a hypoxia incubator (3% O_2, 5% CO_2, 92% N_2) at 37℃ for 24h.

Plasmids and siRNAs

siRNAs were constructed by RiboBio (Guangzhou, CN). Plasmids were constructed by genomeditech (Shanghai, CN). Lipofectamine 3000 (Invitrogen) are used during transfection according to the manufacturer's protocol. pDsRed2-Mito is designed for fluorescent labeling of mitochondria. The vector can be introduced into mammalian cells which the mitochondrial targeting sequence is from subunit VIII of human cytochrome c oxidase. The Mito sequence is fused to the 5'-end of DsRed2, the Mito sequence targets the Mito-DsRed2 fusion protein to the host cell's mitochondria.

Renal function measurement

Blood samples were centrifuged at 3000 rpm for 15 min at room temperature. Urine was collected by metabolic cages, then centrifuged at 3000 rpm for 15 min at 4 ℃. Serum creatinine were measured by an assay based on the Jaffe method (Nanjing Jiancheng Bioengineering Institute, CN). Urea nitrogen were assessed by commercial kits (Nanjing Jiancheng Bioengineering Institute, CN) according to the manufacturer's instructions.

Quantification of mRNA by quantitative real-time PCR

Total RNA was extracted using TRIzol Reagent (Invitrogen, No.15596026) according to the manufacturer's instructions. First strand cDNA synthesis was performed using PrimeScript™ RT reagent Kit (Perfect Real Time) (TAKARA, No. RR047A). qRT-PCR was performed using TB Green® Premix Ex Taq™ II (TAKARA, No. RR820L) on Roche 480II as following: 95˚C for 30s to denaturation, then 40 cycles of 95˚C for 5 s, followed by 60˚C for 30s to PCR, 95˚C for 5s and 60˚C for 1 min, followed by 95˚C to melt, finally 50˚C for 30s to cool down. All the experiments were performed in triplicates. Relative amounts of mRNA for targeting genes were normalized to β-actin. All the sequences of the primers are shown in Table S1.

The $2^{-\Delta\Delta CT}$ method was used in real-time PCR.

$\Delta CT(test) = CT(target) - CT(ref)$; $\Delta CT(calibrator) = CT(target) - CT(ref)$; $\Delta\Delta CT = \Delta CT(test) - \Delta CT(calibrator)$;   Fold change$=2^{-\Delta\Delta CT}$.

Quantification of mitochondrial DNA copy numbers

Total DNA was extracted using Genomic DNA Mini Preparation Kit with Spin Column (Beyotime, No. D0063) and relative mitochondrial DNA (mtDNA) and nuclear DNA (nDNA) were determined by qRT-PCR with D-Loop 2 gene to represent mtDNA and G6PC gene to represent nDNA. The mtDNA

copy numbers were indicated by the ratio of mtDNA to nDNA. The following primers were used: D-Loop 2: F-GGCTCTCAACTCCAGCATGT; R- AGGACGAGGGAGGCTACAAT; G6PC: F-CTGTCTTTGATTCCTGCCTCAT; R- GTGGCTGTGCAGACATTCAA.

The information of D-loop, hypervariable region 2 which is located in <u>D-loop</u> complement (join(1..576)) was found in NCBI and the primers were designed with the following sequence.

Forward primer   CTGTCTTTGATTCCTGCCTCAT;

Reverse primer   GTGGCTGTGCAGACATTCAA.

Western blotting

After treatment, cells were harvested in RIPA buffer containing protease and phosphatase inhibitor Cocktail, and nuclear proteins were extracted using Nuclear Extraction Kit (ab113474, Abcam, Cambridge, MA). Protein concentration was determined using BCA Protein Assay kit (Solarbio, PC0020). 25–50 μg proteins were loaded on a 10 % Tris-Tricine SDS gel. After electrophoresis, proteins were transferred to 0.45 μm PVDF or 0.22 μm nitrocellulose membrane and were incubated with primary antibodies as shown in Table S1 at 4˚C overnight. The signal was detected using peroxidase-conjugated species-specific secondary antibodies and visualized by enhanced chemiluminescence (ECL, Millipore, WBKLS0500) on a Storm 860 phosphorimager (Molecular Devices).

Co-immunoprecipitation

The Co-immunoprecipitation was performed using Co-IP kit (Thermo Scientific Pierce#26149) following the manufacturer's instructions. Briefly, HK-2 cells were cultured in 60 mm dishes and approximately 1 mg cell lysates were incubated with 10 μg MRPL12 or SQSTM1/p62 antibody immobilized Amino Link Plus coupling resin at 4°C overnight, with rabbit-IgG cross-linked resin as a negative control. After washing, the proteins were eluted using elution buffer and were analyzed by western blotting.

Immunofluorescence staining

Cells were washed with PBS then fixed in 4% PFA for 15 min at room temperature. After washing three times with PBS, cells were permeabilized in 0.1% Triton X-100 in PBS for 10 min and blocked for 1 h at room temperature by 1% goat serum (Solarbio, SL038). The cells were then incubated with primary antibodies (Table S1, 1:200) overnight at 4 °C, followed by three washes in PBS and incubation with secondary antibody (Table S1) for 1h at room temperature. Nuclei were counterstained with Hoechst 33342 (Life technologies, H3570). Images were obtained by LSM 700 Laser scanning confocal

microscope (Zeiss, Germany) and Nikon microscope imaging system (Nikon Ti-S, Tokyo, Japan) and analyzed by Image J. Briefly speaking, the cell slides were scanned with same exposure time and intensity and each group contents three biological repetitions.

Mito-DsRed2 fluorescent labeling

For mitochondrial staining, the Mito sequence targets the Mito-DsRed2 fusion protein to the host cell's mitochondria. The total number of cells analyzed in overexpressed group and vector group keep generally consistent which were probably 24 while in group knockdown cells and scramble cells were probably 15. The presented intensity is calculated as fold of the intensity per pixel. The fluorescence intensity of pDsRed2-Mito per se was analyzed by Image-Pro Plus 6.0.

In situ proximity ligation assay (in situ PLA)

SQSTM1/p62 knocked down and scramble control cells were fixed in 4% paraformaldehyde and permeabilized in 0.1% Triton X-100. The PLA assay was carried out according to manufacturer's instructions (Duolink, MilliporeSigma) with rabbit monoclonal anti-p38 (Abcam Cat# ab32142) and mouse monoclonal anti-SQSTM1/p62antibodes (Abcam Cat# ab56416). The signal was visualized using an imageXpress confocal microscope (Molecular Devices) and analyzed by Image J.

Immunohistochemistry

Kidneys were fixed in paraformaldehyde for 24h, dehydrated and embedded in paraffin. 5μm sections were cut and stained with hematoxylin and eosin, or prepared for immunohistochemistry staining after antigen retrieval. Slides were incubated with the primary antibodies (p62, MRPL12, ND1, CYTB, COXII, ATP8) overnight at 4 °C, followed by secondary antibody incubation (Zhongshan, CN) for 1h, and visualized by avidin-biotin complex (Vector Labs). The images were acquired with a Nikon microscope imaging system (Nikon Ti-S, Tokyo, Japan) and analyzed by NIS element software.

Bioenergetic profile analysis

The bioenergetic profiles of the cells were analyzed by an XF96 extracellular flux analyzer (Seahorse Biosciences, North Billerica, MA, USA) as described. Briefly, the cells in 4 replicates were seeded in XF96 Cell Culture Microplates and changed medium into unbuffered, serum-free DMEM (Seahorse Biosciences, North Billerica, MA, USA) supplemented with 10mM glucose, 10mM pyruvate, and 2mM glutamine (Agilent Technologies, CA, USA). After incubated in a non-CO_2 incubator for 1 hour, the oxygen consumption rate was measured in a time course before and after the injection of oligomycin (2 μM), FCCP (Carbonyl cyanide-4-(trifluoromethoxy) phenylhydrazone, 1 μM), and rotenone/antimycin

A (5 μM).

Chromatin Immunoprecipitation (ChIP) assay

ChIP assays were performed using a ChIP assay kit (Merck, No. 10086) according to the manufacturer's instructions. In brief, chromatin was crosslinked with 1 % formaldehyde (Sigma) at room temperature for 10 minutes, and stopped by the addition of glycine to a final concentration of 125mM. Chromatin was then sonicated and immunoprecipitated with antibodies against ATF2 with rabbit IgG as control. Real-time PCR was performed with primers that amplified human MRPL12 promoter containing a putative ATF2 binding site identified from ALLGEN PROMO.

Electrophoretic mobility shift assay (EMSA)

The Gel Shift Chemiluminescent EMSA kit was used (Active Motif 37341). ATF2 binding motifs were labeled with biotin at the 5' end (sense: CACATCTGACGTCTTCTCAC; antisense: GTGAGAAGACGTCAGATGTG) (Integrated DNA Technologies). For competition tests, a mutated probe (sense: CACATCCAGTACTCCCTCAC; antisense: GTGAGGGAGTACTGGATGTG) and cold probe of the same sequence was added to the reaction mixture at 200x excess. The reaction was incubated for 30 min at room temperature, and then loaded on a 6 % retardation gel. The contents of the gel were transferred to a nylon membrane, and visualized with the chemiluminescent reagent as recommended.

Luciferase activity

An MRPL12 firefly luciferase reporter plasmid was constructed with wild type or mutant ATF2 binding site, and was co-transfected into HK-2 cells with p62 overexpressing shRNA using Lipofectamine® 3000 (Invitrogen). Luciferase activity was measured using the dual-luciferase reporter assay system (Promega, E1910) on Centro XS LB 960 (Berthold, Thoiry, France).

Electron microscopy

The electron microscopy procedure was performed as described previously (Wei et al, 2015). In brief, kidneys were dissected and rapidly fixed in ice-cold 2.5 % glutaraldehyde, dehydrated by dimethylketone. After embedding, all samples were cut into ultrathin sections and dyed with uranium acetate and plumbum citrate. Images were acquired on JEM-100sX electron microscopy and mitochondrial numbers were counted using Image-Pro plus 6.0.

Oxygen consumption measurements

Oxygen consumption of mitochondria from renal cortex in WT and CKO mice was measured by Clark-type oxygen electrodes containing a magnetic stirrer (Hansatech Instruments, Norfolk, U.K.). Briefly,

0.2 g renal cortex tissue was ground to extract mitochondria. Oxygen consumption was recorded after adding substrates and inhibitors for Complex I (5mM Glutamate plus 5mM Malate, 2mM Rotenone), Complex II + III (5mM Succinate, 0.1mM Antimycin A) and Complex IV (1.2mM TMPD, 6mM KCN). Detailed procedure is according to the manufacturer's instructions.

Mass spectrometry-based proteomics

Differentially expressed genes with statistical significance between the two groups were identified through Volcano Plot filtering. The experiment consists of three sets of biological replicates. A total of 47 proteins were identified with a 95 % confidence interval in SQSTM1/p62 knocked down TECs and scramble siRNA transfected control cells. genes were chosen for further data analysis such as clustering, GO, KEGG pathway, and protein interaction.

Statistical analysis

Statistical data was expressed as mean ± standard deviation (Mean ± SD). Each experiment was performed at least for three times, the statistical analysis of the data was performed using t-tests or One-Way ANOVA followed by Sidak's multiple comparisons test built in GraphPad Prism (GraphPad Software 5.0; San Diego, CA). For two groups comparison, the Student's t-test was used with homogeneity of variance, and the t´ test was used with heterogeneity of variance. For multiple groups comparison, One-Way ANOVA was used with homogeneity of variance and the Welch method is used with heterogeneity of variance; Differences with $P < 0.05$ were considered statistically significant. *$P<0.05$, **$P<0.01$, ***$P<0.001$.

Supplemental References

Yang, B., Lan, S., Dieude, M., Sabo-Vatasescu, J. P., Karakeussian-Rimbaud, A., Turgeon, J., Qi, S., Gunaratnam, L., Patey, N. and Hebert, M. J. (2018). Caspase-3 Is a Pivotal Regulator of Microvascular Rarefaction and Renal Fibrosis after Ischemia-Reperfusion Injury. J Am Soc Nephrol. *29*, 1900-1916.

Xin W, Zhao X, Liu L, Xu Y, Li Z, Chen L, Wang X, Yi F and Wan Q. (2015). "Acetyl-CoA carboxylase 2 suppression rescues human proximal tubular cells from palmitic acid induced lipotoxicity via autophagy" J Biochem Biophys Res Commun. *463*, 364-9.